Universidade de Aveiro Departamento de Química
2019

DIOGO ESTEVES PEREIRA

MAGNETIC IRON OXIDE FUNCTIONALIZATION OF WASTE-BASED ACTIVATED CARBON FOR THE REMOVAL OF CARBAMAZEPINE FROM WATER

FUNCIONALIZAÇÃO DE CARVÃO ATIVADO COM ÓXIDOS DE FERRO MAGNÉTICOS PARA A REMOÇÃO DE CARBAMAZEPINA DA ÁGUA

Universidade de Aveiro
2019

Departamento de Química

DIOGO ESTEVES PEREIRA

FUNCTIONALIZATION OF WASTE-DERIVED ACTIVATED CARBON FOR THE REMOVAL OF CARBAMAZEPINE FROM WATER

FUNCIONALIZAÇÃO DE CARVÃO ATIVADO COM ÓXIDOS DE FERRO MAGNÉTICOS PARA A REMOÇÃO DE CARBAMAZEPINA DA ÁGUA

Dissertação apresentada à Universidade de Aveiro para cumprimento dos requisitos necessários à obtenção do grau de Mestre em Biotecnologia Industrial e Ambiental, realizada sob orientação científica da Doutora Vânia Maria Amaro Calisto, Investigadora Auxiliar do Departamento de Química da Universidade de Aveiro, e do Doutor Valdemar Inocêncio Esteves, Professor Auxiliar do Departamento de Química da Universidade de Aveiro.

Cofinanciado por:
COMPETE 2020
PORTUGAL 2020
UNIÃO EUROPEIA
Fundo Europeu de Desenvolvimento Regional
FCT Fundação para a Ciência e a Tecnologia
MINISTÉRIO DA CIÊNCIA, TECNOLOGIA E ENSINO SUPERIOR

Apoio financeiro da FCT e COMPETE2020 no âmbito do projeto de investigação WasteMAC - POCI-01-0145FEDER-028598

o júri

presidente

Doutora Sónia Patrícia Marques Ventura

Professora Auxiliar do Departamento de Química da Universidade de Aveiro

Doutora Cláudia Batista Lopes

Investigadora do Departamento de Química da Universidade de Aveiro

Doutora Vânia Maria Amaro Calisto

Investigadora Auxiliar do Departamento de Química da Universidade de Aveiro

agradecimentos

À minha orientadora, Vânia Calisto, pela oportunidade de trabalhar diariamente num grupo de investigação ímpar do qual me fez sentir parte desde o primeiro dia. Agradeço todo o conhecimento partilhado e a incansável disponibilidade e paciência.

Ao Professor Valdemar Esteves por todas as sugestões, críticas e pelas palavras de incentivo.

Às minhas colegas de laboratório por toda a ajuda e boa disposição.

Ao Doutor Nuno Silva (CICECO, UA) e à Doutora Maria Victoria Gil Matellanes (INCAR-CSIC, Oviedo) pelo apoio na caracterização dos materiais.

Ao Engenheiro Milton Fontes e funcionários da “Águas do Centro Litoral” pela cedência de efluentes.

Um agradecimento especial aos meus pais, à minha família e amigos pelo apoio incondicional.

Keywords Activated carbon, Industrial wastes, Pyrolysis, Magnetic nanoparticles, Adsorption, Pharmaceuticals, Environment, Wastewater treatment

Abstract

Adsorption of pharmaceuticals onto activated carbons constitutes one of the most promising technologies for the removal of these persistent contaminants from water. Production of activated carbon from wastes provides an alternative and eco-friendlier option to commercial non-renewable-based activated carbon and simultaneously contributes to the valorisation of industrial and agricultural biomass residues that enforces the principles of a circular economy. However, the application of powdered activated carbon in continuous treatment systems is hampered by the difficulty in recovering the material from the treated aqueous phase. The loading of magnetic iron oxide nanoparticles onto the surface of the activated carbon can facilitate the recovery of the adsorbent by the application of an external electromagnetic field or a permanent magnet, avoiding expensive and complex processes such as filtration or coagulation.

In this work, magnetic activated carbon (MAC) was produced *via* two synthesis pathways. Waste-based powdered activated carbon (WPAC) produced from primary paper mill sludge (PS) was used as precursor in both routes. The *in-situ* route involves the coprecipitation of magnetic iron oxides onto the surface of WPAC. The *ex-situ* route involves the separate production of magnetic iron oxide particles, subsequently added in suspension to WPAC, at controlled pH.

The produced materials were physically and chemically characterized (total organic carbon, Fourier transform infrared spectroscopy, specific surface area, pore morphology, point of zero charge, vibrating sample magnetometer, scanning electron microscopy imaging and X-Ray diffraction) and subject of preliminary adsorption tests for the removal of the anti-epileptic carbamazepine (CBZ) from ultrapure water. Best materials were selected (*in-situ* MAC2-MP1 and *ex-situ* MACX1-MP1), and kinetic and equilibrium studies were performed in both ultrapure water and real effluent collected from a local wastewater treatment plant. Kinetic studies revealed that equilibrium was achieved at around 30-45 min for both materials in both matrices. Maximum adsorption capacities for CBZ in ultrapure water were 90 ± 4 mg g^{-1} and 121 ± 5 mg g^{-1}, for MAC4-MP1 and MACX1-MP1, respectively. In real effluent maximum adsorption capacities were lower for both materials, 60 ± 3 mg g^{-1} and 78 ± 2 mg g^{-1} for MAC4-MP1 and MACX1-MP1, respectively. Both materials presented lower adsorption capacities than the non-magnetic WPAC. However, magnetization was successfully achieved in both cases and the materials proved to be competitive with a non-magnetic commercial PAC in ultrapure water, which indicates to a potential application in continuous water treatment systems.

Palavras-chave Carvão ativado, Resíduos industriais, Pirólise, Nanopartículas magnéticas, Adsorção, Fármacos, Ambiente, Tratamento de águas residuais

Resumo

A adsorção de fármacos a carvões ativados é uma das tecnologias mais promissoras para a remoção destes compostos persistentes da água. A produção de carvões ativados a partir de resíduos de biomassa constituí uma alternativa mais barata e ecológica aos carvões ativados produzidos a partir de precursores não-renováveis, permitindo a valorização de resíduos industriais e agrícolas e aplicando os valores de uma economia circular. No entanto, a aplicação de carvões ativados em pó em sistemas de tratamento em contínuo é inibida pela dificuldade de separação do material das águas residuais tratadas. O carregamento de nanopartículas magnéticas de óxido de ferro na superfície do carvão ativado facilita a recuperação pela aplicação de um campo eletromagnético externo ou um íman permanente, evitando processos dispendiosos como a filtração ou a coagulação.

Neste trabalho, carvões ativados magnéticos (MAC) foram produzidos por duas vias. Um carvão ativado derivado de resíduos (WPAC) produzido a partir de lamas primárias da indústria papeleira (PS) foi usado como precursor. A via de produção *in-situ* envolve a coprecipitação de óxidos de ferro magnéticos diretamente na superfície do WPAC. A via *ex-situ* envolve a síntese em separado dos óxidos de ferro magnéticos e subsequente adição ao WPAC em suspensão a pH controlado.

Os materiais produzidos foram alvo de caracterização física e química (carbono orgânico total, espectroscopia de infravermelho com transformada de Fourier, área superficial específica, morfologia dos poros, ponto de carga zero, *vibrating sample magnetometer*, microscopia de varrimento eletrónico e difração de raios-X) e sujeitos a testes de adsorção preliminares para a remoção do antiepilético carbamazepina (CBZ) de água ultrapura. Os melhores materiais foram selecionados (*in-situ* MAC4-MP1 e *ex-situ* MACX1-MP1) e sujeitos a testes de cinética de adsorção e de isotérmica, tanto em água ultrapura como em efluente real recolhido numa ETAR local. De acordo com os estudos cinéticos, ambos os materiais atingiram o equilíbrio entre os 30-45 min em ambas as matrizes. As capacidades máximas de adsorção em água ultrapura foram de 90 ± 4 mg g^{-1} e 121 ± 5 mg g^{-1}, para MAC4-MP1 e MACX1-MP1, respetivamente. Em efluente real as capacidades máximas de adsorção foram inferiores para ambos os materiais, 60 ± 3 mg g^{-1} e 78 ± 2 mg g^{-1} para MAC4-MP1 e MACX1-MP1, respetivamente. Ambos os materiais apresentaram capacidades de adsorção inferiores ao WPAC. Contudo, a sua magnetização foi atingida com sucesso e os materiais provaram ser competitivos com um PAC não-magnético comercial em água ultrapura, o que indica a sua potencial aplicação em sistemas de tratamentos de água em contínuo.

Contents

List of figures

List of tables

Abbreviations

AC	Activated carbon
ASS	Absolute sum of squares
ATR	Attenuated total reflectance
BET	Brunauer-Emmett-Teller
CBZ	Carbamazepine
CE	Capillary electrophoresis
CEC	Chemicals of emerging concern
CSTR	Continuous stirred-tank reactor
CZE	Capillary zone electrophoresis
D	Average pore width
DOC	Dissolved organic carbon
DWTP	Drinking water treatment plant
EKC	Electrokinetic capillary chromatography
EOF	Electroosmotic flow
FTIR	Fourier transform infrared spectroscopy
GAC	Granular activated carbon
HPLC	High performance liquid chromatography
IC	Inorganic carbon
LOD	Limit of detection
LOQ	Limit of quantification
MAC	Magnetic activated carbon
MEKC	Micellar electrokinetic chromatography
MP	Magnetic iron oxide particles
OC	Organic carbon
PAC	Powdered activated carbon
PS	Primary paper mill sludge
PZC	Point of zero charge
S_{BET}	Specific surface area

SEM	Scanning electron microscopy
TC	Total carbon
TOC	Total organic carbon
V_p	Total pore volume
VSM	Vibrating sample magnetometer
W_0	Micropore volume
WPAC	Waste-based powdered activated carbon
WWTP	Wastewater treatment plant
XPS	X-ray photoelectron spectroscopy
XRD	X-ray diffraction

I. Introduction

1 | Pharmaceuticals as emerging contaminants

The scarcity of water resources and the increasing environmental awareness along with the necessity for protection of natural ecosystems have lead many countries to introduce remediation and treatment technologies in national wastewater management plans [1]. However, conventional wastewater treatment processes tend to fail in the complete elimination of low concentration and recalcitrant contaminant compounds [2,3], whose long term and continuous exposure may cause known or suspected negative impacts in human health and ecological systems. These compounds, often called chemicals of emerging concern (CEC), are not commonly monitored and comprehend a broad group of chemicals for which regulatory criteria or quality standard is usually absent [4].

The Directive 2013/39 EU of the European Union reviews the list of priority substances in the field of water policy for which it establishes environmental quality standards. It also states the need for stimulation of the development of new, cheaper and more cost-effective water treatment technologies and it reports the lack of monitoring data for emerging pollutants currently not included in monitoring programmes in the European Union but that may pose a risk and thus, require regulation [5]. This Directive was complemented by the Decision 2015/495/EU and, more recently, by the Decision 2018/840/EU where several pharmaceuticals were included in the watch-list of compounds with environmental relevance [6,7].

1.1 | Pharmaceutical production, consumption and disposal

Among the CEC, pharmaceuticals are a broad and diversified group of compounds, produced massively worldwide, with the aim of preventing, treating or curing diseases and improving human and animal health. The global consumption of this type of highly active molecules is of the order of hundreds of tons annually [8]. The increasing world population along with greater life expectancy, the advances in pharmaceutical and medical research, the increasingly prevalence of chronic diseases and the expiration of drug production patents, are all factors contributing for growing pharmaceutical consumption and production [8,9]. It is estimated that approximately 3200 substances are used as pharmaceutically active compounds [10], including antibiotics, lipid regulators, analgesics, anticonvulsants, beta-blockers, antidepressants and antidiabetics.

Pharmaceuticals are a distinct group of substances which possess some characteristics that differentiate them from conventional industrial chemical contaminants [11]:

- Vast range of molecular weight, structure and functionality;
- Polar, lipophilic molecules with degrees of ionization and properties dependent on the pH of the medium;
- High persistence in the environment (in some cases, more than a year; some may reach several years and become biologically active through accumulation);
- Susceptible to chemical structure modification upon ingestion and absorption.

Due to the rising production and consumption, pharmaceuticals are found in the environment, mainly aquatic, more recurrently in concentrations in the few ng L^{-1} to μg L^{-1} [12,13]. Rehman and co-workers have identified several risks of global pharmaceutical contamination from highly populated developing countries which hold a large pharmaceutical industry. These substances and its transformation products end up permeating several environmental matrices, posing a threat not only for those countries but also for their exportation destinations [14]. Figure 1 schematizes some of the possible pharmaceutical substances' routes to enter the aquatic environment.

Significant amounts of pharmaceutical drugs are excreted in unmetabolized form, or as conjugates, usually inactive but capable of reassuming the parent compound form after hydrolysis, or as other metabolites (active or inactive) into sewage and wastewater treatment systems. Most pharmaceuticals undergo metabolic transformation before being excreted, during which reactions of oxidation, reduction or hydrolysis take place, often producing metabolites that could be more reactive and toxic than the parent compound [15]. Wastewater treatment plants (WWTP) effluents are directly discharged to water bodies or reused for irrigation and biosolids production; therefore, pharmaceutical metabolization and excretion followed by WWTP ineffective processing is considered the primary pathway of pharmaceutical compounds into the environment [16–19].

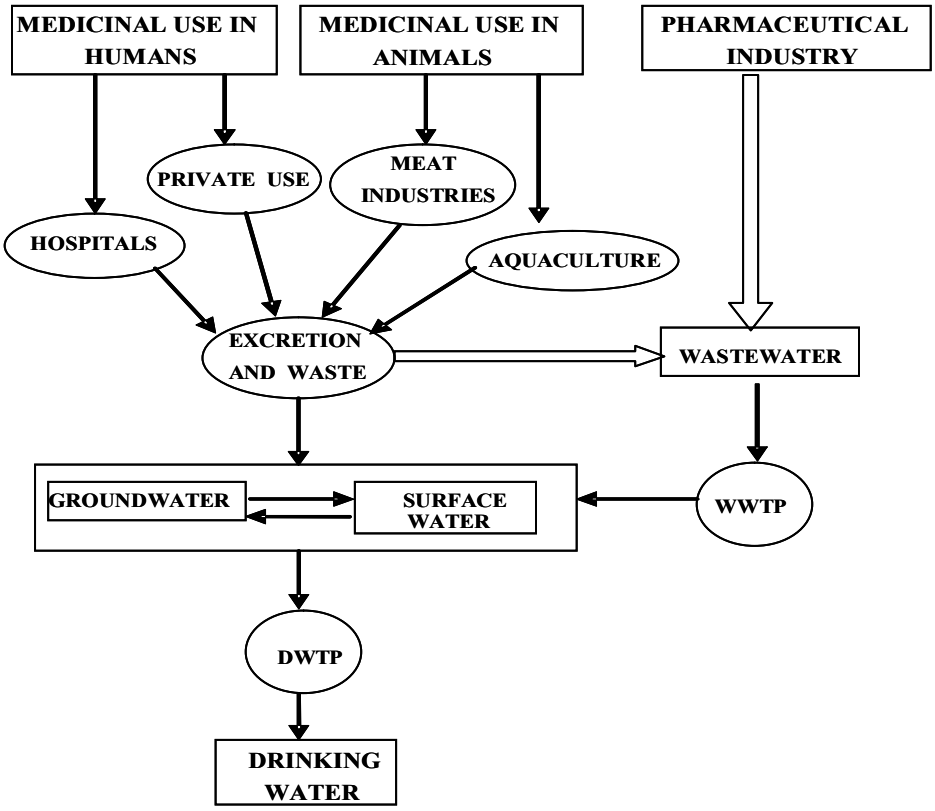

Figure 1 – Pharmaceutical compounds main entry routes in the aquatic environment [11]

Pharmaceuticals used in veterinary medicine, mainly in intensive livestock production, are either excreted into the ground, eventually reaching groundwater, or directly introduced into surface waters without passing through a WWTP, while in aquaculture, pharmaceutical compounds are directly disposed in surface waters [11]. Pharmaceutical production and processing facilities are also potential major contributors for water body contamination. Most manufacturers lack active monitorization of effluents with several studies suggesting these sites as important source of active pharmaceutical compounds, creating stresses in WWTP and aggravating the risk of aquatic contamination [20–24]. Alternative routes such as skin washing of topically applied pharmaceuticals, sweat excretion or incorrect unused pharmaceutical disposal may also constitute important entry pathways of pharmaceuticals into the environment [18].

1.2 | Pharmaceutical occurrence and ecotoxicological risk

Pharmaceuticals have been detected in surface and ground waters in several countries around the world [11,25,26]. Table 1 lists the mean concentration of different pharmaceuticals detected in river and marine coastal waters in countries located in the Mediterranean basin, namely Spain, Italy, Greece, France, Turkey, Israel and others [26]. These substances end up reaching ground water repositories from various sources, which rises concern since these depositories are the main source of drinking water in many countries [27]. In fact, some pharmaceuticals are found in drinking water supply systems at low concentrations [28,29], with no significant acute toxicity but potential long term exposure toxic effects.

In 2017, the occurrence of 23 pharmaceuticals, from 6 therapeutic groups, in Portuguese surface waters was assessed [30]**.** Several samples were collected in geographically distinct surface waters upstream and downstream of selected WWTP, along two different seasons. The study revealed the occurrence of 11 pharmaceuticals, with up to 8 pharmaceuticals present per sample. The maximum concentration of 69.2 ng L^{-1} was detected for the analgesic paracetamol. Selective serotonin reuptake inhibitors, commonly used as antidepressants, were found to be the therapeutic group present in highest average concentration, followed by anti-inflammatories, antibiotics, antiepileptics and lipid regulators. Surprisingly, downstream samples showed an increase of pharmaceutical concentration of 20.7%, which suggest a negative impact of WWTP in Portuguese surface waters.

Although present in relative low concentration in the environment [13,25] and below levels of acute toxicity, several pharmaceutical compounds raise concerns about potential ecotoxicological hazards, whether as single compounds or as part of a complex mixture [31]. Depending on the composition of the mixture, pharmaceuticals, metabolites and transformation products may act independently, synergistically (worsen their toxic effect) or antagonistically (compensating toxic effects of each other) [32]. In some cases, metabolites may represent greater risk in water environment than the parent drug. In a recent study, the environmental exposure concentrations in surface water were predicted for 24 selected pharmaceuticals and their metabolites. The results indicated that 18 metabolites, from 12 of the parent compounds, have greater eco-toxicity and hazard quotients, and may pose greater risk than the original drug [33].

Table 1 – Mean concentrations of pharmaceuticals detected in rivers and seawaters in the Mediterranean basin (Adapted from [26])

Class of pharmaceutical	Substance	Rivers (ng L^{-1})	Seawaters (ng L^{-1})
Analgesic anti-inflammatory	Diclofenac	238	6,1
	Ibuprofen	257	13,9
	Naproxen	243	2
	Acetaminophen	249	219
	ketoprofen	85	0,02
Lipid Regulator	Bezafibrate	218	2,1
	Gemfibrozil	336	4,4
	Clofibric acid	188	0,12
Psychotropic drug	Carbamazepine	237	0,32
	Fluoxetine	8	< LOD
β-blocker	Propanolol	20	2,2
	Atenolol	77	32,8
	Sotalol	134	24,6
Antibiotic	Sulfamethoxazole	167	1,9
	Clarithromycin	166	10,4

< LOD: below the limit of detection

Several studies suggest potential adverse impacts related with environmental and human toxicity of pharmaceuticals and mixtures at environmentally relevant concentrations [34]. For instance, the exposure to a mixture of 13 commonly detected pharmaceuticals inhibited zebrafish liver cells proliferation in vitro [35]. The effects involved transcriptional changes of genes largely involved in primary metabolism and regulation of the cell cycle, among others. The results were consistent with a previous work by the same author, where human embryonic cells were exposed to the same mixture of pharmaceuticals at environmental exposure levels (ng L^{-1}) [36]. The highest effect observed was a 30% decrease in cell proliferation when compared to controls. In another study, the exposure of rainbow trout female to a mixture of pharmaceuticals at concentration levels identical to those measured in river water caused an increase of the plasma level of sex hormones and the overexpression of genes encoding for key enzymes in steroidogenesis and ovary maintenance [37].

1.3 | WWTP pharmaceutical removal

The occurrence of pharmaceutical substances in several environmental matrices downstream of WWTP is, in part, justifiable by their inefficient capacity to eliminate these compounds and corresponding metabolites and transformation products. Most conventional WWTP procedures involve a primary physical and chemical treatment followed by a secondary biological treatment, usually in the form of activated sludge, which tends to result in limited removal capacity since most pharmaceutical compounds are not metabolized by microorganisms and may even inhibit their activity [11]. Degradation rate and efficiency greatly depend on the structure and functional groups of the compound, and complete removal is very difficult to achieve [38].

A 3-year study, analysing samples of influent and effluent fluid streams from 7 different WWTP, evaluated the removal efficiency of 73 pharmaceuticals [39]. Results showed poor or no elimination for the anti-epileptic carbamazepine (CBZ), generally presenting higher concentrations in effluent streams, which may result from conversion of CBZ conjugates to the parent compound. Substances like lipid regulators, tetracycline antibiotics and beta-blockers were partially degraded (40-70% removal efficiency). High removal efficiencies were registered for non-steroidal anti-inflammatory drugs with values between 81-99% removal. In another study, CBZ and several of its metabolites had little to no degradation when subjected to conventional wastewater treatment [40]. CBZ was found at both influent and effluent wastewater at concentrations around 2 $\mu g\ L^{-1}$, with some of its metabolites being found with concentrations as high as 3-4 $\mu\ L^{-1}$.

Several other studies report the incomplete liquid phase removal of various pharmaceuticals [16,41–43]. Therefore, the development of alternative and sustainable remediation technologies capable of greater performances is of the utmost importance.

2 | Adsorption

Among tertiary wastewater treatment methods such as ozonation, chlorination, membrane filtration, or UV treatment, adsorption by activated carbons (AC) has showed great potential in the elimination of micropollutants, like pharmaceuticals, from WWTP secondary effluents [17].

Adsorption is the accumulation of a substance (adsorbate) at a surface or interface (adsorbent). It occurs when a solid surface is brought into contact with a liquid or gas, generating interactions between the fields of forces of both phases. The adsorbate tends to accumulate near the solid adsorbent surface as a result of the retention of molecules, atoms or ions from the adsorbate phase. There are two types of adsorption, depending on the nature of the forces involved. In physical adsorption, the adsorbate is reversibly bound to the surface by relatively weak non-electrostatic forces, mainly van de Waals forces but also hydrophobic interactions and hydrogen bonds. On the other hand, when adsorption occurs through electrostatic forces is named chemical adsorption and might involve redistribution and exchange of electrons between the adsorbate molecules and the adsorbent surface (chemisorption), producing a much stronger interaction than that of physical adsorption [44].

The two types of adsorption, chemisorption and physisorption, greatly differ in the magnitude of the enthalpy of adsorption, being of the order of 40-400 KJ per mol and 10-20 KJ per mol, respectively. Besides, physical adsorption is non-specific and may occur between any adsorbate-adsorbent system, whereas chemisorption is much more specific. The thickness of the adsorbed phase is also different in the two types. In chemisorption, it forms a unimolecular layer and in physical adsorption a multimolecular one. The type of adsorption that takes place in a given adsorbate-adsorbent system, as well as adsorption rate and efficiency, depends on the nature of the adsorbate, the nature of the adsorbent, the reactivity of the surface, the surface area of the adsorbate, and the temperature and pressure of adsorption [44,45].

For the purpose of this work, only liquid-solid adsorption will be addressed in the following sections, as the objective is to evaluate the adsorptive performance of carbon adsorbents for drug removal in aqueous systems.

2.1 | Adsorption isotherms

Considering adsorption from dilute solutions, the process starts with a high adsorption rate due to the greater adsorbent surface available for interaction. As the adsorbent's surface becomes saturated with adsorbate molecules, adsorption rate decreases and the reverse process of desorption initiates. From a kinetic point of view, the system reaches a state of equilibrium when adsorption and desorption rates are equal [44,46]. But adsorption equilibrium can also be described as the dynamic balance between the concentration of solute adsorbed and the concentration of solute left in the bulk solution, which is established once the adsorbate has been in contact with the adsorbent for enough time [47]. In that sense, adsorption isotherms are employed to represent the equilibrium relationships of an adsorption system. Overall, they are functions that describe the retention (or release) and mobility of a liquid-phase adsorbate in solid-phase adsorbent at constant temperature and pH. Adsorption isotherms are essential for the determination of important parameters, such as adsorption capacity, which are the basis for the evaluation and selection of the best adsorbents for a particular application [46,47].

Adsorption isotherms are also used, for instance, in the case of physical adsorption of gases on porous carbons, to determine surface area (Brunauer-Emmett-Teller (BET) equation [48]) and volume, size and distribution of pores (Dubinin-Radushkevich equation [49]).

Considering a single component liquid-phase system, where solvent adsorption is neglected and only solute adsorption is accounted, the equilibrium adsorption capacity, q_e (mg g^{-1}), is given by the mass balance relationship (Equation (1)):

$$q_e = \frac{(C_0 - C_e)V}{m} \tag{1}$$

where C_0 and C_e are the initial and equilibrium liquid-phase concentrations of adsorbate (mg L^{-1}), respectively, V is the volume of solution (L) and m is the mass of adsorbent used (g) [46,50].

The mathematical correlations underlined by the adsorption isotherms constitute an important role in modelling analysis, operational design and applicability of adsorption systems [47]. In this context and along with the determination of adsorption equilibrium parameters, such as adsorption capacity, the evaluation of the adsorption capacity over

time is of the utmost importance. An ideal adsorption system comprises both high adsorption capacity and fast kinetics. The following sections analyse both these factors.

2.1.1 | Adsorption equilibrium models

The shape of the isotherm is the first indicator of the nature of the adsorption process and is used to classify the most common types. Several adsorption isotherms have been formulated and commonly appear on the literature. In the scope of this work, mainly five types are described for carbon materials, which are the linear type, type L (Langmuir), type F (Freundlich), type H (High affinity) and type S (Sigmoid) isotherms (Figure 2).

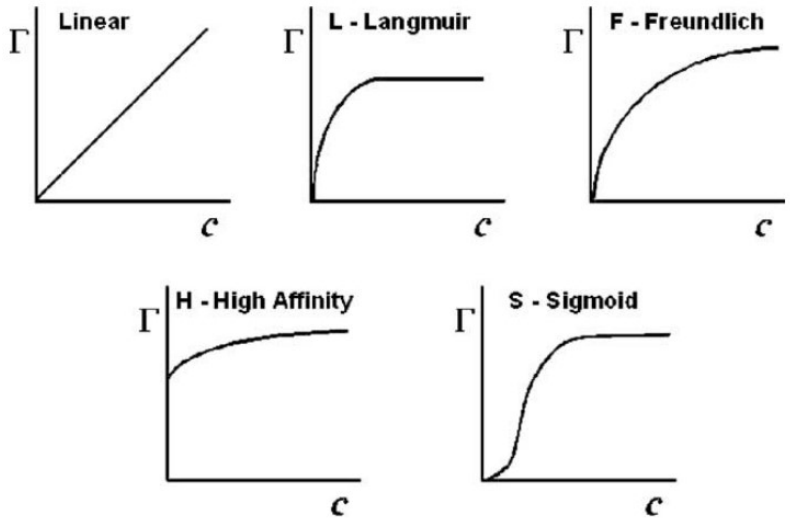

Figure 2 – Common adsorption isotherms found in liquid-phase adsorption onto carbon materials [46]

Type L isotherm curves occurs in the majority of adsorption from dilute solutions [51] and is typically observed for porous materials [52]. The probability of the solute finding a suitable site for adsorption progressively decreases as less sites are available, which can explain the saturation (*plateau*) at high solute concentrations that characterize this monolayer isotherm type and also the later stages of S and H types. For this reason, it is hypothesized that the solute is adsorbed non-vertically and that there is no considerable competition from the solvent [51,52]. As for the initial part of S type curves, commonly obtained for homogenous surfaces, the adsorption of solute is facilitated by neighbouring adsorbed molecules because of lateral cooperative interactions. As a result, adsorption is favoured as concentration of solute increases [51]. Type H isotherms differ quantitatively

from type L, as the solute molecules demonstrate such high affinity for the adsorbent that virtually no solute can be detected in the liquid-phase and the initial stages of the curve are characterized by a vertical line [52]. Type F isotherms can be considered as a type L isotherm. They are usually associated with heterogenous surfaces, which have regions of high and low adsorption affinity [52]. The simplest isotherm is the linear type, where adsorption of solute is described by a linear increase.

There are several mathematical models which describe the referred isotherm patterns. The experimental adsorption data is usually correlated with well-known adsorption isotherm models to find the best fitting model. The isotherm's parameters are usually used to predict the system performance for a specific adsorbent and adsorbate pair. Some examples of adsorption isotherm model are given by the Langmuir and Freundlich equations.

2.1.1.1 | Langmuir isotherm model

The Langmuir model is based on the assumption that adsorption occurs in a monolayer with one solute molecule of thickness and at a fixed number of defined and localized binding sites that are energetically equivalent. It is also considered that there are no lateral interactions between adsorbed molecules and all adsorption sites have equal affinity for the adsorbate [44,47]. Equation (2) mathematically describes the single component non-linear Langmuir adsorption model:

$$q_e = \frac{q_m K_L C_e}{1 + K_L C_e} \tag{2}$$

where q_e (mg g^{-1}) refers to the equilibrium adsorption capacity, q_m (mg g^{-1}) is the maximum adsorption capacity, K_L (L mg^{-1}) is the Langmuir equilibrium constant and C_e (mg L^{-1}) is the concentration of solute in the aqueous phase at equilibrium.

The Langmuir model is graphically characterized by a *plateau* corresponding to the attainment of solute equilibrium saturation in the monolayer, from which point no further adsorption takes place. From the model equation it is possible extrapolate the maximum adsorption capacity for the specific solute (q_m). Additionally, a dimensionless constant referred to as separation factor (R_L) can be defined by the Equation (3):

$$R_L = \frac{1}{1 + K_L C_0} \quad (3)$$

where C_0 (mg L^{-1}) is the initial concentration of solute. From R_L constant value, adsorption for a specific adsorbent-adsorbate pair can be considered unfavourable ($R_L > 1$), linear ($R_L = 1$), favourable ($0 < R_L < 1$) or irreversible ($R_L = 0$) [47].

2.1.1.2 | Freundlich isotherm model

The Freundlich model describes a non-ideal and reversible adsorption process, usually applied to heterogenous systems [47]. Contrarily to the Langmuir model, both monolayer and multilayer adsorption can be described by this model. According to its mathematical formulation, the concentration of solute adsorbed is favoured with the increase in solute concentration. This relation implies that no defined state of equilibrium is attained, hence no maximum adsorption capacity can be derived from its formulation. Equation (4) describes the non-linearized form of the Freundlich model, which is typically applied in dilute solution systems:

$$q_e = K_F C_e^{1/n} \quad (4)$$

where K_F ($mg^{1-1/n}$ $L^{1/n}$ g^{-1}) is the Freundlich equilibrium constant and n is a constant related with non-linearity of the equation and is commonly used as measure of the intensity of the adsorption, so that if $n = 1$ the adsorption is linear, if $n > 1$ adsorption is favourable and if $n < 1$ adsorption is non-favourable [47].

2.2 | Adsorption kinetic models

As previously mentioned, adsorption kinetics is a fundamental parameter in the design of any adsorption system. It is critical to evaluate the solute uptake rate, which determines the residence time required for the completion of the adsorption process [53]. For that purpose, several models can be applied although, in the scope of this work, two models are briefly described in the following sections, namely the pseudo-first order and pseudo-second order adsorption kinetic models.

2.2.1 | Pseudo-first order model

The pseudo-first order kinetic model was firstly presented to describe a liquid-solid adsorption system and it proposes that the solute uptake rate is directly proportional to the difference between the quantity of solute adsorbed at equilibrium and at a given time (t):

$$\frac{d_q}{d_t} = k_1(q_e - q_t) \quad (5)$$

where k_1 is the pseudo-first order rate constant (min^{-1}), q_e (mg g^{-1}) is the adsorption capacity at equilibrium and q_t (mg g^{-1}) is the adsorption capacity at a certain time t [53]. The model's non-linear form is given by Equation (6):

$$q_t = q_e[1 - exp(-k_1 t)] \quad (6)$$

2.2.2 | Pseudo-second order model

This model is based on the assumption that adsorption is described by a second order equation and that chemical adsorption, involving valent forces, is the rate limiting step [53]. The pseudo-second order is mathematically described by Equation (7) or, in its non-linear form, Equation (8):

$$\frac{d_q}{d_t} = k_2(q_e - q_t)^2 \quad (7)$$

$$q_t = \frac{k_2 q_e^2 t}{1 + k_2 q_e t} \quad (8)$$

where k_2(g mg^{-1} min^{-1}) is the pseudo-second order rate constant of adsorption.

2.3 | Activated carbon

Activated carbons (AC) are amorphous materials mainly characterized by their extensive porous structure and large surface area. Generally, AC are characterized as having specific surface area (S_{BET}) most commonly between 800 and 1500 m^2 g^{-1} and a pore volume in the order of 0.20-0.60 cm^3 g^{-1} [44].

This type of material is mainly composed of carbon, with its typical elemental composition being 88% C, 0.5% H, 0.5% N, 1% S, and 6 to 7% O (oxygen content may

vary in the range of 1-20%, depending on precursor material and activation process), and inorganic ash representing the remaining fraction [44], which usually blocks the pores and thus, should be as low as possible. Because of carbon unique bonding properties, both with other elements and itself, three major allotropic forms of carbon may occur: diamond, graphite and fullerenes. The graphite form is a parallel layered graphene structure maintained by dispersive and van der Waals forces (Figure 3).

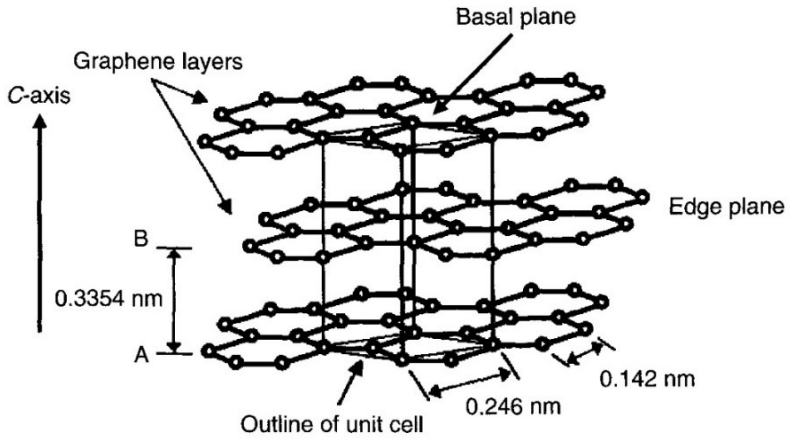

Figure 3 – The structure of graphite [45]

Activated carbons are a form of non-graphitic carbons which means that no crystallographic order is present in the structure apart from the roughly parallel graphene layer stacking. Non-graphitic carbons include graphitizable and non-graphitizable carbons. A non-graphitizable carbon is a non-graphitic carbon which cannot be transformed into graphitic carbon (measurable crystallographic order) by high temperature treatment under atmospheric or lower pressure, being able to present a complex porous microstructure (Figure 4) [45,54]. Thus, AC are non-graphitic, non-graphitizable carbons with a highly disordered microstructure (Figure 4 (b)).

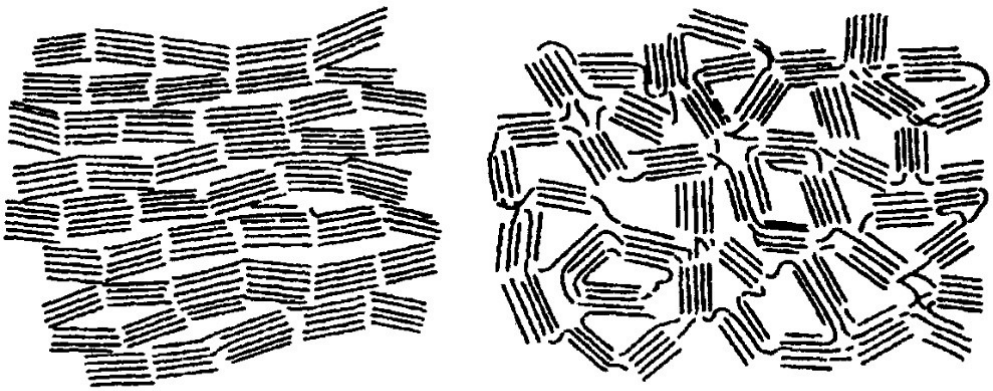

Figure 4 – Illustration of the essential differences between graphitizable and non-graphitizable carbon [45]

As defective assemblies of graphene layers, AC are associated with pores starting from less than a nanometre to several thousand nanometres. Such pores can be classified, according with their diameter, as micropores (< 2 nm), mesopores (2-50 nm) and macropores (> 50 nm). In micropores, most of the adsorption takes place due to the overlapping adsorption forces in near opposing walls. Typically, micropores' surface might constitute up to 95% of the total AC surface area, whereas mesopores does not exceed 5%. However, mesopores contribute significantly to the adsorption by functioning as guiding entrances, conducting the adsorbate to the micropores. On the other hand, macropores influence in the adsorption process is not considerable [44].

Adsorption takes place both on planar surfaces of the carbon structure, through van der Waals forces, and on the edges of those planes, through more specific chemical bonding. Carbon atoms located at the edges of the basal graphene planes (Figure 2) are unsaturated and contain unpaired electrons. Most of these sites are bonded to heteroatoms (atoms other than carbon) which give rise to diverse functional groups. Surface functional groups have tremendous impact on adsorption. Among these groups, oxygen-containing surface groups are the most common and important ones (Figure 5), capable of influencing surface characteristics such as polarity and acidity, and other properties such as chemical, catalytical and electrical reactivity of these materials. For example, aromatic compounds (commonly present in organic molecules) can be adsorbed at the carbonyl oxygens on the carbon surface. These groups act as the electron donor, while the aromatic ring of the adsorbate acts as the electron acceptor [44,54,55].

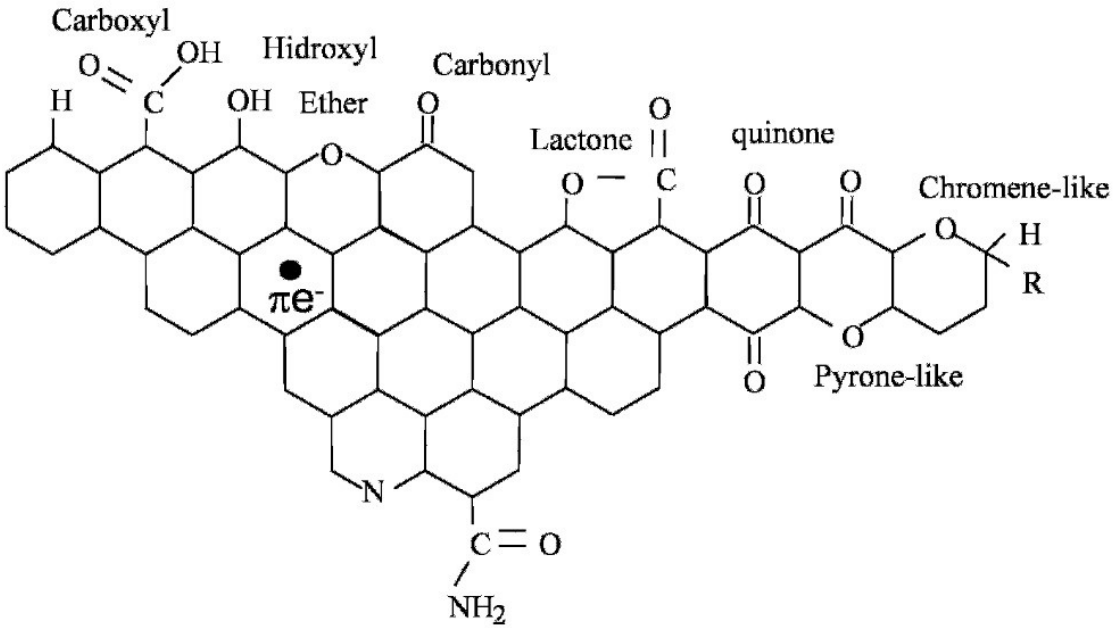

Figure 5 – Some of the most common and important functional groups found in AC [54]

Functional groups, especially oxygen-containing surface groups, may demonstrate acidic or basic behaviour depending on the pH of the medium. Thus, if the pH > PZC (point of zero charge of the AC), protons are released into the medium, leaving a negatively charged surface on the carbon. On the other hand, if the pH < PZC, basic sites combine with protons from the medium and reinstate a positively charged surface [54].

2.3.1 | Production of activated carbons

The conventional production of AC involves two main steps: carbonization and activation. Carbonization or pyrolysis is the thermal degradation of a carbon-rich precursor in an inert atmosphere (usually N_2), with total or partial devolatilization of the raw material, giving rise to pore formation. The activation phase may be of two types, chemical or physical. Physical activation methodologies generally consist of initial pyrolysis of the raw material at medium to high temperatures to produce a carbon rich char, followed by partial gasification at high temperature with an oxidizing agent such as water steam, carbon dioxide (CO_2), oxygen (O_2) or mixture of them [56,57]. Chemical activation is usually carried out in a single step, where the precursor is impregnated with a specified amount of chemical agent and subsequently pyrolyzed at medium-high temperature (450-1000ºC) depending on the chemical agent and raw material [54]. Common chemical agents used are phosphoric acid (H_3PO_4), zinc chloride ($ZnCl_2$),

potassium carbonate (K_2CO_3) or an alkali hydroxide, such as potassium hydroxide (KOH) [58–61]. After pyrolysis, the porous structure remaining may be filled with inorganic residual matter, such as ash, or its pores may be obstructed by disoriented carbon. Washing the resulting material with acid unblocks the pores and is followed by a thorough wash with distilled water.

The type and composition of the raw material, and the carbonization conditions heavily influence the morphology of the porous matrix. The activation process is a key step in increasing both volume and diameter of the pores [44]. Chemical activation is usually preferred over physical activation due to lower activation temperature and time, yielding lower energy consumption, better development of the porous structure, with higher surface area. Some disadvantages of chemical activation processes are the requirement of a following washing step and the corrosion of the equipment, due to the nature of the chemical agents [54].

Currently, commercially available AC is mainly produced from fossil fuels, such as bituminous coal, and wood [54]. However, such process is limited by availability, due to the unrenewable nature of the carbon source and cost. Powdered (PAC) and granular (GAC) activated carbons are currently applied in the field of water treatment. Their use depends on its specific application. For instance, PAC has the advantageous feature of presenting greater S_{BET} when compared to GAC. On the other hand, GAC shows greater regeneration capability by thermal or chemical processes over PAC since its particle size allows for the use in continuous processes without compromising reusability. PAC, however, is usually used in batch mode due to its lower particle size, which increases difficulty of separation in continuously stirred reactors [45].

As an alternative, several agricultural and industrial wastes have been studied as precursors for the production of AC, with the major benefits being the renewable nature of the carbon source, the reduced process costs and availability of the precursors [62]. The valorisation of these wastes constitutes a sustainable form of waste management, which becomes more important in the context of a circular economy. Table 2 shows some examples of AC production from renewable waste sources using chemical activation. Several nut shells, fruit stones, sugarcane and beet bagasse and various residues from the cereal production, among many others, have already been used for the production of AC [62–64].

Table 2 – Alternative precursors to produce AC

Precursor	Chemical Agent	Pyrolysis Temperature (ºC)	S_{BET} (m^2 g^{-1})	Reference
Rice husk	K_2CO_3	950	1260	[65]
Cotton stalks	KOH	700	997	[66]
Corn cob	$ZnCl_2$	500	767	[67]
Wood shavings	H_3PO_4	450	812	[68]
Paper mill sludge	KOH	800	1627	[69]
Bleached paper pulp	H_3PO_4	800	965	[70]
Hazelnut shells	KOH	600	1700	[71]

Sludge from the pulp and paper industry has been investigated as precursor for the production of carbon adsorbents, including AC, and subsequent potential application in pharmaceutical removal from water [69,70,72–80]. In a recent study, the reproducibility of the use of paper mill sludge for the production of adsorbents was assessed by evaluating the impact on the final product characteristics of the variability over time of sludge batches and the variability between sludges from two different factories with different pulp and/or paper production processes [72]. Results showed a lack of consistency in the materials produced from sludge precursors of different factories, which was associated with the distinct production operation, and from biological paper mill sludge. However, good reproducibility was found in the materials produced from different batches of primary paper mill sludge (PS) for each factory. These findings show good reliability for potential use of these industrial residues as precursors to produce carbon adsorbents.

A 2017 study compared the single and multi-component adsorption capacity of a non-activated carbon for the removal of three psychiatric drugs from water, produced using PS, with a commercial AC [80]. The PS was pyrolyzed at 800 ºC in a N_2 atmosphere (similarly to [77]) subsequently washed with HCl, obtaining an S_{BET} of 414 m^2 g^{-1}, lower than the commercial AC used as reference (848 m^2 g^{-1}). It was concluded that single pharmaceutical maximum adsorption was higher for the commercial adsorbent, but the single maximum adsorption was reduced for both cases in a multi-component system, which might indicate competition between the analysed pharmaceuticals. Nevertheless, it was obtained a porous carbon material with approximately half the S_{BET} of a commercial AC without resorting to any activation method.

A more promising result was achieved when PS was impregnated with a chemical agent prior to pyrolysis [69]. A full factorial experimental design analysed parameters like pyrolysis temperature (650 and 800ºC) and residence time (60 and 150 min), type of activating agent (K_2CO_3 and KOH) and impregnation ratio (10:1 and 1:1 precursor:activation agent mass ratios). The study concluded that the main factors affecting the S_{BET} and the analysed pharmaceutical adsorption efficiency were the pyrolysis temperature and impregnation ratio. The materials produced following optimal conditions (AC 3, 4, 6 and 7 - Figure 6) showed, in general, suitability for the adsorption of the selected pharmaceuticals (sulfamethoxazole, CBZ, and paroxetine) from water, with adsorption efficiencies and S_{BET} values much higher than the commercial AC used as reference (PBFG4 (Chemviron) – Figure 6). Best results were obtained for PS impregnated with KOH in a mass ratio of 1:1 and pyrolyzed at 800 ºC for 150 min, then washed with HCl and water to remove inorganic matter (S_{BET} = 1627 m^2 g^{-1}).

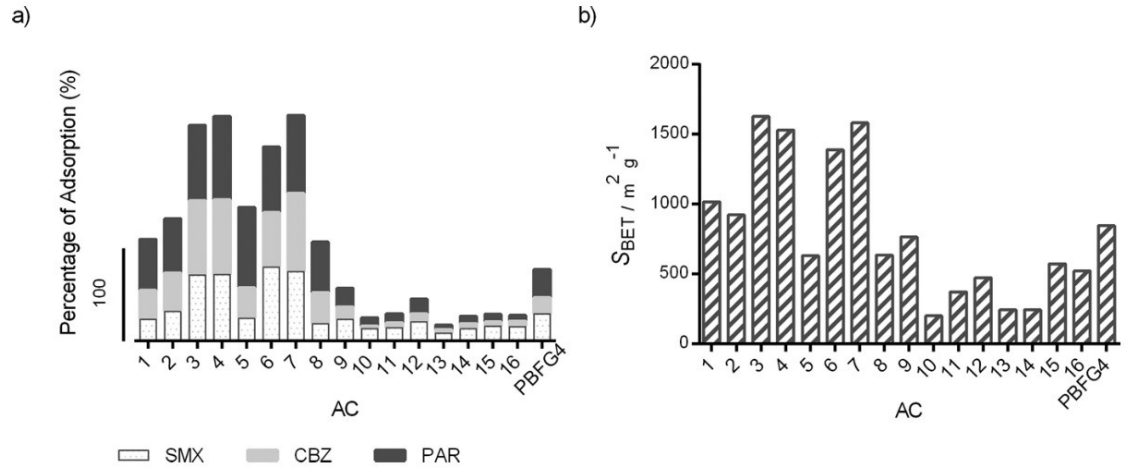

Figure 6 – a) Percentage of adsorption of the analysed pharmaceuticals (SMX – sulfamethoxazole; CBZ – carbamazepine; PAR - paroxetine) and b) S_{BET} for the produced (AC1-16) and commercial (PBFG4) AC [69]

2.3.2 | Magnetic nanoparticle loading onto carbon adsorbents

Conferring magnetic properties to carbon absorbents provides a simple and inexpensive mechanism of separation of such adsorbents from the treated aqueous phase. Through the application of a magnetic field, magnetic adsorbents and the retained adsorbates are sequestered, and the treated media can be released. Such process would eliminate the need of costly and time-consuming separation processes such as coagulation/flocculation, filtration, centrifugation or slow sedimentation [81]. The allocation of magnetic

properties to AC would be particularly advantageous in the application of PAC in continuous adsorption processes, for instance a continuous stirred-tank reactor (CSTR), since its smaller particle size facilitates magnetic aggregation and separation.

2.3.2.1 | Magnetic iron oxides

Several metallic precursors can be used to impart magnetic properties to carbon adsorbents, such as iron (Fe), nickel (Ni) and cobalt (Co) based compounds. Due to the relative low cost, high availability and the capacity to introduce great magnetic properties, iron based compounds are usually preferred, specially iron salts [82]. Iron oxide nanoparticles are the most used nanoparticles for the magnetization of carbon adsorbents. There are 16 distinct iron oxide species in the form of oxide, hydroxides and oxyhydroxides. Magnetite (Fe_3O_4) and maghemite (γ-Fe_2O_3) are the oxide forms that present greater ferrimagnetic properties at room temperature [83]. Magnetite, the most magnetic of both, is a crystalline oxide with cubic structure of inverse spinel type composed of a mixture of ferric (Fe^{3+}) and ferrous (Fe^{2+}) iron, while maghemite, with identical structure, is mainly composed of Fe^{3+}. Maghemite can be considered a fully oxidised magnetite [84], and the distinction between the two iron oxide magnetic phases is difficult through x-ray diffraction (XRD) analysis, but possible by x-ray photoelectron spectroscopy (XPS).

Synthetic formation of iron oxide particles in the micron and submicron range usually takes place in aqueous systems, through processes of nucleation and crystal growth. The most commonly used methods for the preparation of magnetite involve oxidative hydrolysis of Fe^{2+} salts [84] or coprecipitation of Fe^{2+}:Fe^{3+} solutions. Temperature, addition of an alkali agent and the provision of an inert atmosphere of N_2 are fundamental parameters to ensure a faster and more efficient precipitation. Other aspects, such as concentration of iron precursor, pH of the suspension and the presence of foreign ion species are controlling parameters that affect the purity and morphology of the iron oxide precipitate obtained [84].

The oxidative hydrolysis of ferrous salts involves the partial oxidation of a Fe^{2+} salt solution with an oxidizing agent, generally KNO_3, under alkaline environment and inert atmosphere. Temperature is fundamental in defining magnetite particle size (lower sizes for lower temperatures) and pH must be kept constant and above pH>8 to obtain higher

yields and crystalline magnetite [84]. Co-precipitation is a similar but simpler and more commonly used process in the context of production of AC with magnetic properties. Magnetite synthesis through chemical coprecipitation is a simple and efficient mechanism for the formation of magnetic nanoparticles in which a base is added, usually dropwise, to an aqueous iron salt solution (Fe^{2+} and Fe^{3+}), under an inert atmosphere, at temperatures under 100ºC. This method does not produce or use any toxic intermediates or solvents, being advantageous for its eco-friendliness and easy scale-up [85]. Coprecipitation is initiated by a nucleation increment when the concentration of the iron species reaches critical supersaturation which is followed by the slow growth of the newly formed nuclei and diffusion of solutes to the surface of the crystal [86]. The mechanism of magnetite formation through coprecipitation has been well investigated [85,87]. Magnetite is formed by phase transformation of intermediate iron oxyhydroxides, rather than direct reaction of the Fe^{2+} and Fe^{3+} species. As pH gradually increases with the addition of base, several iron oxide phase transformations occur in the following manner: akageneite → goethite → hematite → maghemite → magnetite [85]. Coprecipitation is a complex multi-reaction process and, therefore results in a broad magnetite nanoparticle size distribution and low particle crystallinity [85]. The most widely used iron salt precursors are $FeCl_2$, $FeSO_4$, $FeCl_3$, $Fe(NO_3)_3$. The selection of the iron salt precursor, specifically the corresponding anion, influences the size of the magnetite nanoparticle. Although, it apparently shows no interference with the nanoparticle morphology, bigger precursor anions result in smaller magnetite particle size [87].

2.3.2.2 | Magnetic activated carbon

The loading of AC with magnetic nanoparticles to produce magnetic activated carbons (MAC) has been object of recent studies. The literature also presents several examples when the subject of magnetization is a non-activated carbon (biochar) [86,88,89].

There are two main routes for the production of MAC. The one step route consists of simultaneous activation and magnetization, which means that impregnation with activating agent and iron precursor occurs prior to pyrolysis [90,91]. The two step route involves the production of AC followed by loading of magnetic nanoparticles through chemical precipitation of magnetite. The magnetization can occur by two ways that distinguish themselves by the presence or not of the AC during the coprecipitation

reaction. The *in-situ* route involves the coprecipitation of magnetic iron oxides directly onto the surface of AC by adding it to the reaction medium, whereas the *ex-situ* method implies that the coprecipitation occurs independently and the AC is later suspended with the produced magnetic particles at controlled pH to promote electrostatic interaction. An alternative way involves a physical process called ball milling, in which AC and magnetic nanoparticles are mixed in a rotating cylinder filled with spheres [92]. Table 4 presents some examples of MAC obtained via two step coprecipitation process, from different iron precursors, and different AC types derived from both biomass and coal (commercial). The two step approach is the most referred method in the literature and presents less experimental challenges due to the greater control over the process of synthesis magnetic nanoparticle, as opposed to the one step approach.

Table 3 – MAC produced by two step coprecipitation magnetization processes

AC precursor source	Metallic precursor	Temperature (ºC)	Alkali agent	S_{BET} ($m^2\ g^{-1}$)	Reference
Rice straw	$FeSO_4$ + $FeCl_3$	70	NaOH	674	[93]
Coconut shell commercial	$FeSO_4$ + $FeCl_3$	60	NaOH	951	[94]
Coconut shell commercial	$FeSO_4$ + $FeCl_3$	50	NH_3	516	[95]
Coal-based commercial	$FeCl_3$ + $FeCl_2$	80	NH_3	1241	[96]
Coal-based commercial	$FeSO_4$ + $FeCl_3$	70	NaOH	658	[97]

In 2002, one of the first MAC reported in the literature was produced through the impregnation of a commercial AC (S_{BET} = 933 $m^2\ g^{-1}$) with a solution of $FeCl_3$ and $FeSO_4$ (400 mL; Fe^{3+}:Fe^{2+} molar ratio 2:1) at 70 ºC [97]. Coprecipitation was carried out through the dropwise addition of 100 mL NaOH 5 M solution. The obtained materials were dried at 100 ºC for 3 h. The AC:iron oxide weigh ratios tested were 1:1, 2:1, 3:1. The materials obtained revealed high magnetic responsiveness when in proximity with a magnet. An overall decrease in S_{BET} (658 $m^2\ g^{-1}$) and micropore volume was observed. Analysis revealed that the main magnetic iron oxide phase formed was maghemite, followed by a small amount magnetite. Bulk sigma magnetization analysis of the pure iron oxide, without the AC, under the same conditions, revealed values close to those of maghemite.

Besides, the pure iron oxide formed revealed a Fe^{3+}:Fe^{2+} ratio much higher than the one found in the original impregnation solution which might indicate the formation of Fe^{3+} rich iron oxide species, such as maghemite. XRD analysis also suggest the presence of small amounts of goethite and hematite, which are known non-magnetic iron oxide intermediates in the co-precipitation of magnetite [85].

In another study [93], MAC was synthesized from rice straw based AC (S_{BET} = 1334 m^2 g^{-1}) through coprecipitation of iron salt precursors, similar to [97]. A certain mass of AC (40% of the weight of iron salts) was impregnated in a 200 mL $FeCl_3$:$FeSO_4$ solution (Fe^{3+}:Fe^{2+} molar ratio 2:1) at 70 ºC, and subsequent addition of 100 mL NaOH 5 M solution, under vigorous stirring. The mixture was aged for 3 h at the referred temperature, allowed to cool and the material was thoroughly washed with distilled water. The resulting MAC (S_{BET} = 674 m^2 g^{-1}) presented superparamagnetic behaviour, which implies easy recovery under an external magnetic field or magnet. Besides obvious S_{BET} reduction, the waste-based MAC showed a decrease in total pore volume and micropore volume, suggesting the precipitation of iron oxide particles inside the pore structure of the MAC [93]. XRD analysis indicates that the main crystalline iron oxide phases formed were goethite, maghemite and magnetite. The magnetic adsorbent was tested for the adsorption of triclosan, a common antibacterial and antifungal agent present in detergents, from water. The rice straw based MAC revealed a maximum adsorption capacity of 303 mg g^{-1}, which is significantly lower than the precursor AC (714 mg g^{-1}), and greater sensitiveness to the pH medium than the AC [93].

In a different study, magnetite nanoparticles were synthetized individually by coprecipitation and later added in suspension to HNO_3 pre-treated commercial AC (S_{BET} = 1378 m^2 g^{-1}) to produce MAC with good adsorption properties for the removal of CBZ from effluent wastewaters [96]. The HNO_3 pre-treatment is a chemical oxidation process that implants oxygen containing functional groups, such as carboxyl, carbonyl and hydroxyl groups, onto the surface of the AC [95]. The objective was to reduce the PZC of the AC to create a pH interval where AC and magnetic nanoparticle had opposite surface charge, generating electrostatic attraction. Therefore, the PZC of AC was reduced to pH=2, while the PZC of magnetite is usually pH=6, thus in the pH range of 2 to 6 the AC surface is mostly negatively charged, and the magnetite surface is positively charged [96]. Magnetite nanoparticles were prepared similarly to previously described methods, using a $FeCl_3$:$FeCl_2$ solution (molar ratio 2:1) at 80 ºC, under agitation and N_2 flow.

Nitrogen was used to create a non-oxidizing oxygen free environment to prevent further oxidation of magnetite nanoparticles according to the reaction: $Fe_3O_4 + 0{,}25O_2 + 4{,}5H_2O \rightarrow 3Fe(OH)_3$ [98]. The alkali solution (NH_3) was added dropwise and the precipitated magnetic nanoparticles were washed with deoxygenized water. The magnetization process occurred by dispersing magnetic nanoparticles and AC in 500 mL of deoxygenated water, at different mass ratios (1:2; 1:4; 1:8 – magnetite:AC), under stirring and N_2 flow, and subsequently adjusting the pH to 4 to promote the attraction between AC and nanoparticles. After magnet separation and drying, the obtained materials were washed with HCl to remove Fe ions adsorbed onto the AC surface, which could block the pores, and then washed with distilled water and dried again to obtain the final magnetic material. XRD analysis revealed peaks related to standard cubic pattern of magnetite and maghemite. The average magnetite nanoparticle size obtained was 50 nm. Higher magnetite contents were associated with higher saturation of magnetization. Nevertheless, the 1:8 magnetite:AC ratio revealed saturation of magnetization high enough to be separated by an external magnetic field and a slight decrease in surface area (S_{BET} = 1241 $m^2\ g^{-1}$) which might be related to blockage of pores by oxygen containing functional groups and magnetite nanoparticles. It was concluded that magnetite had no adverse impact on the adsorption capacity of the MAC, and a decrease in adsorption capacity with the higher magnetite content could be explained by increase of inactive mass of adsorbent, with relatively neglectable contribution to CBZ adsorption, and not by the negative interference of magnetite. The 1:8 MAC revealed a maximum CBZ adsorption capacity of 182.9 mg g^{-1}, lower than the precursor commercial AC (274 mg g^{-1}), and a maximum removal efficiency of 93% in real effluent wastewaters [96]. These results indicate promising potential for the application of MAC in the refinement of effluent wastewaters.

Besides the introduction of magnetic properties, the iron salt precursor can also act as an activating agent in a one step production of MAC. The production of MAC through impregnation of charred coconut shell (S_{BET} = 6.22 $m^2\ g^{-1}$) with $FeCl_3$ was tested [91]. The carbonized biomass waste was impregnated with $FeCl_3$ at different mass ratios ($FeCl_3$:biomass char) in an aqueous solution, under stirring at room temperature for 2 h, before the water being evaporated in a 120 ºC oven, and the solid residue pyrolyzed at 700 ºC for 1.5 h, acid (HCl) and water washed and dried. Results revealed a decrease of S_{BET} and total pore volume with an increase in the iron salt impregnation ratio, being that

the highest S_{BET} was achieved by the 1:1 impregnation ratio (372 m^2 g^{-1}). All produced MAC presented high saturation of magnetization and superparamagnetic properties at room temperature. XRD and XPS spectra indicated the formation of magnetite, maghemite and hematite iron oxide phases. The authors suggest that the magnetic iron oxide was formed through a series of phase transformations starting by the formation of iron hydroxides through hydrolysis of Fe^{3+} aqueous impregnation medium, to the formation of intermediate iron oxides, such as goethite, maghemite and hematite, in the following steps of evaporation and pyrolysis, and culminating in the formation of magnetite at maximum pyrolysis temperature (700 ºC) [91].

A magnetic non-activated carbon (biochar) was produced through oxidative hydrolysis of a Fe^{2+} salt, and it was tested for the adsorption of sulfamethoxazole from water [99]. For this purpose, a pine sawdust biochar (S_{BET} = 297.8 m^2 g^{-1}) was saturated in a $FeCl_2$ 0.3 M solution for 24 h, under agitation. After that, the mixture was kept at 90 ºC under N_2 flow while a solution of KOH (alkali agent) and KNO_3 (oxidizing agent) were added dropwise for 1 h. The suspension was cooled overnight in an air sealed reactor, and subsequently centrifuged to obtain magnetic biochar, followed by washing with distilled water and drying. The objective of this process was to prevent the formation of iron oxide/hydroxide phases other than nanosized magnetite. XRD analysis substantiated the formation of only magnetic iron oxide forms. Therefore, the material presented high saturation of magnetization, with good retrievability by magnet. The precipitation of magnetic nanoparticles on the surface of the biochar reduced its S_{BET} (125 m^2 g^{-1}), as expected, not only because of plausible pore blockage but also because of the low surface area of the magnetic nanoparticles [99]. The adsorption capacity towards sulfamethoxazole was also reduced (13.83 mg g^{-1}), possibly due to low electrostatic attraction between the pharmaceutical and magnetic adsorbent at the pH tested (pH = 4), at which the adsorbent is mainly positively charged (PZC = 9.46) and the sulfamethoxazole is neutral. It was also concluded that the synthesized magnetic nanoparticles had no sorption affinity to the pharmaceutical.

3 | Basic principles of capillary electrophoresis

Capillary electrophoresis (CE) is a well-established analytical technique for the determination of small molecule pharmaceuticals in water. In this work, CE was used as analytical method for the quantification of the adsorbate concentration remaining in solution after adsorption. Molecule separation occurs due to distinct migration rates, based on analyte charge and size ratio, across a narrow tube (generally a fused-silica capillary) under an applied high constant electric field (Figure 7). This format of electrophoresis provides a relatively simple separation mechanism that allows for rapid analysis with high sample throughput [100]. Additionally, in comparison with high performance liquid chromatography (HPLC), another high resolution separation technique, CE offers some advantages such as the requirement of small sample amounts (few nanolitres), the ability of separation over a wider range of molecular weights and charges, the higher separation efficiency and resolution, the relative inexpensiveness as opposed to the high cost of HPLC columns and the versatility offered by capillaries allowing for easy inner surface manipulation [101].

Reduced capillary inner diameter (5-150 μm) enable the appliance of high electric fields (10-30 kV), by minimizing heat generation and allowing for more efficient energy dissipation, which is responsible for high separation efficiency and resolution and short analysis periods, characteristic of CE [102].

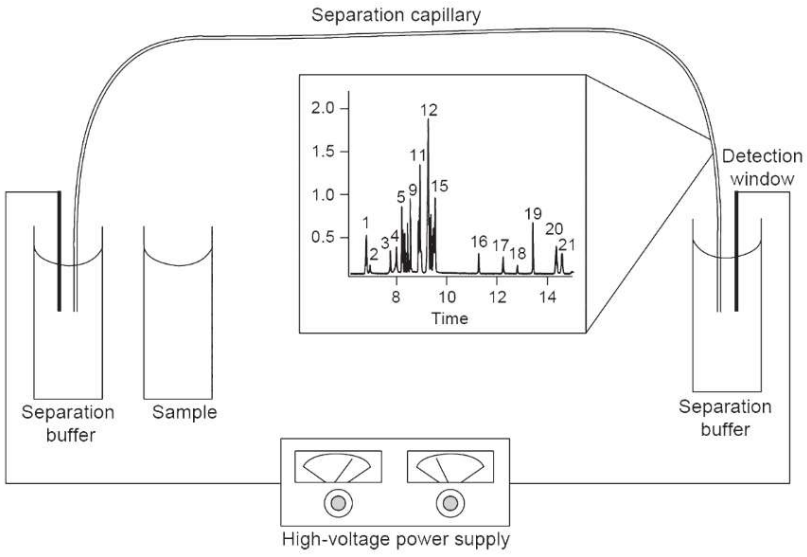

Figure 7 – Schematic representation of a CE instrument [102]

Common to every electrophoretic system, electroosmotic flow (EOF) occurs whenever a fluid (electrolyte) near a charged surface (capillary wall) is placed under an electric field, resulting in the bulk movement of fluid near that surface. EOF is quite a significant factor in CE separations, especially due to the high surface to volume ratio inside the capillary [100]. Manipulation of several experimental variables can be used to modify EOF, such as the type, concentration and pH of the separation buffer, the addition of organic modifiers, temperature or the inner wall composition of the capillary [101]. Another crucial component in CE analysis is the electrophoretic mobility of charged species (analyte) in an electrolyte as a result of the electrostatic force when a constant electric field is applied [101].

Fused-silica capillaries are almost ubiquitous to CE analysis. Their inner surface functionality is determined by silanol groups which bear negative charge at pH=3-9 (common separation condition), thus attracting hydrated cations from the electrolyte solution leading to the formation of an electrical double layer [100,102]. Under an electric field, the loosely bound second cationic layer migrates towards the cathode, dragging along electrolyte solution creating the EOF [101]. The EOF ultimately determines the electrophoretic mobility of the analytes, by influencing their migration velocity depending on whether they move in the same or opposite direction of the EOF [101]; thus, the analyte movement is the sum of the electroosmotic and electrophoretic vectors [100].

CE can be operated in different separation modes being the capillary zone electrophoresis (CZE) the simplest. The separation occurs based on differential electrophoretic mobilities using a background buffered electrolyte. Given that differential migration is only possible for charged species, neutral compounds are carried with the EOF to the detector end (cathode), without separation. Electrokinetic capillary chromatography (EKC) is an alternative separation mode that is based on the introduction of a pseudo-stationary phase into the running buffer, usually by the addition of surfactant. If the concentration of the surfactant is above the critical micellar concentration, surfactant molecules spontaneously from aggregates (micelles) in the aqueous buffer [101]. This separation mode is named micellar electrokynetic chromatography (MEKC) and, although the movement inside the capillary is still controlled by electrokinetic mobility and EOF, the separation is now also based on the partition of the analyte between the micelles and the aqueous phase [101], enabling the separation of both neutral and charged compounds. Analyte molecules

distribute themselves between the hydrophobic interior of the micelles and the aqueous phase based on their polarity. Sodium dodecyl sulphate (SDS) is vastly used as anionic surfactant as it features high water solubility and degree of lipid solubilization power, and low critical micellar concentration (8 mM) [101]. Considering a negatively charged fused silica capillary wall, SDS micelles and EOF have opposite migration directions. However, the net bulk movement direction is dictated by the stronger EOF, towards the cathode on the detector end.

This methodology was applied in this study for the analysis and quantification of CBZ in aqueous solutions. In Calisto (2011) [101], a MEKC method was optimized by dynamically coating the capillary wall, which increases reproducibility of separation by decreasing analyte and capillary wall interactions. The coating procedure is based on the non-covalent bonding of a multiple charged polycation (polybrene) to the deprotonated silanol groups of the capillary wall, followed by coating with a double layer of SDS molecules, establishing a highly negatively charged surface [101]. SDS was also incorporated into the running buffer.

4 | Main goals of the study

Adsorption onto PAC provides an efficient alternative to complement conventional WWTP treatments for the removal of persistent micropollutants. However, due to its small particle size, the application of PAC in continuous water treatment systems is limited and its separation from the treated aqueous phase involves complex, expensive and time consuming processes.

In that sense, the main goal of the present work was to develop and optimize the production of a magnetically retrievable PAC, derived from an industrial waste (primary paper mill sludge), that combines high adsorption capacity with immediate separation from the treated aqueous phase by a permanent magnet.

The aim of this work was to produce a MAC that was effective in the removal of pharmaceuticals from water and for that purpose, the anti-epileptic CBZ, commonly found in aquatic environments and known to be resistant to conventional WWTP treatments, was chosen to evaluate the adsorption performance. Chemical and physical characterization of the produced MAC through total organic carbon (TOC) determination, Fourier transform infrared spectroscopy with attenuated total reflectance (FTIR-ATR) and XRD analysis, PZC and S_{BET} determination, vibrating sample magnetometer (VSM) analysis and scanning electron microscopy (SEM), was also a key objective in this study, allowing to better understand the impact of the materials' properties in the adsorptive performance. Additionally, it was intended to perform adsorption kinetic and equilibrium studies for the best materials in both ultrapure and WWTP effluent, and subsequent kinetic and isotherm modelling of the adsorption process. The use of WWTP effluents for the adsorption tests is intended to evaluate the performance of the developed materials in high complex real matrices.

Overall, it was purposed to maximize CBZ adsorptive removal while guaranteeing rapid and effective MAC separation from the aqueous phase.

II. Materials and Methods

1 | Production of primary paper mill sludge-based powdered activated carbon

Primary sludge from paper mill industry (PS) was used as precursor for the preparation of a waste-based powdered activated carbon (WPAC). The preparation procedure was selected according to optimal conditions determined by [69]. PS was collected from a pulp and paper pulp factory, using eucalyptus wood (*Eucalyptus globulus*) as raw material and an elemental chlorine free bleaching method. After drying, PS was grinded (with a blade mill) and chemically activated with KOH 1:1 (*w/w*) for 1 h under ultrasonic agitation, at room temperature. Batches of 15 g of PS were impregnated with 15 g of KOH (BChem) in 50 mL of distilled water. Following the activation period, the slurry was allowed to dry at room temperature in the fume hood under weak air stream flow. The impregnated material was subsequently pyrolyzed in porcelain crucibles at 800 ºC in a convection furnace muffle for 150 min of residence time with a heating rate of 10 ºC min^{-1}, under constant nitrogen flow through the entire process.

After pyrolysis, the carbonized material was subjected to an acidic washing step, using 1.0 M HCl (37%, Fluka) in a 3% (*w/v*) proportion for 1 h. The mixture was vacuum filtered through a 0.45 µm filter to remove the acid and successively washed with distilled water and filtered until the filtrate reached neutral pH. The WPAC was dried at 100ºC overnight and grinded into a fine homogenous powder using a pestle and mortar.

The overall production yield (Equation (9)) was calculated.

$$\eta(\%) = \frac{final\ mass\ of\ WPAC\ (g)}{mass\ of\ PS\ (g)} \times 100 \quad (9)$$

2 | Production of magnetic activated carbon

Powdered waste-based MAC was produced via two synthesis routes. Both routes involved the coprecipitation of mixtures of Fe^{2+} and Fe^{3+} salts with an alkali solution. On a first approach, the produced WPAC was introduced in the reaction media prior to coprecipitation. This preparation method was named *in-situ* route. Alternatively, magnetic particles were synthesized independently and later added in solution at controlled pH to the WPAC, constituting the *ex-situ* route.

2.1 | Magnetic particles

Magnetic iron oxide particles (MP) were synthesized via coprecipitation of mixtures of iron III chloride hexa-hydrated (>99%, $FeCl_3.6H_2O$, Chem-Lab, Belgium) and iron II sulphate 1.5-hydrated (>99%, $FeSO_4.1.5H_2O$, Chem-Lab, Belgium) with potassium chloride (KOH, BChem, Portugal). Distilled water used in the coprecipitation was previously deoxygenized for 1 h under nitrogen bubbling. Different proportions of iron salt mixtures were tested; 1.5 g of each considered mixture were dissolved in 50 mL of deoxygenized water, in a water bath at 70-80 ºC, under N_2 flux (Figure 8 – a)). After complete dissolution, 50 mL of a 0.5 M KOH solution, also prepared using the deoxygenized water, was added dropwise and the reaction was held during 1 h, keeping the temperature at 70-80 ºC (Figure 8 – b)). The black precipitate was magnetically decanted to remove the excess of alkali solution and washed successively with distilled water until neutral pH (Figure 8 – c)), after which the particles were dried in a convection oven at 40 ºC, overnight or until completely dry, and mechanically grinded.

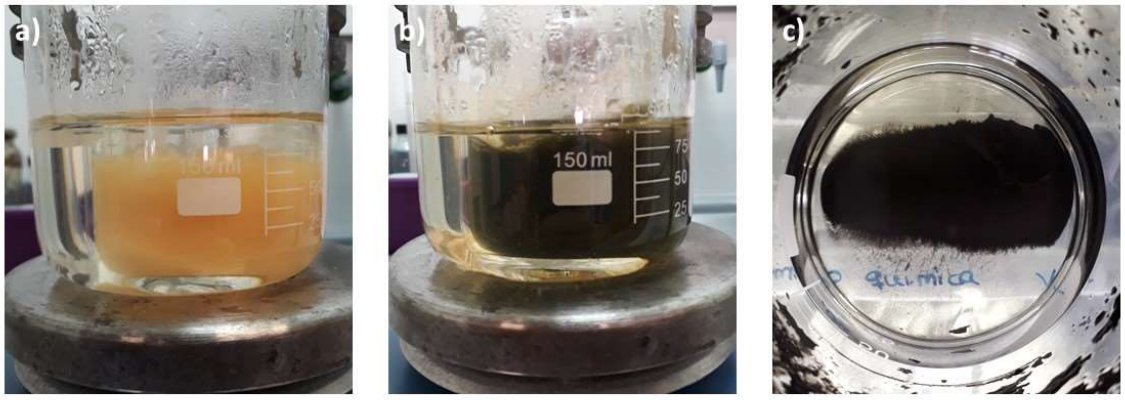

Figure 8 – Coprecipitation reaction: a) iron salt mixture dissolution; b) KOH solution addition; c) final magnetic black precipitate accumulated around a permanent magnet

Magnetic properties of the produced particles were initially evaluated by visual responsiveness to a permanent magnet. For reference, the neodymium rod shaped magnet used (1 cm diameter; 4 cm height) has 1.26-1.29 T (tesla) of residual magnetism, compared to the earth's magnetic field (50 μT), a refrigerator magnet (5 mT), a junkyard magnet (1 T) or a laboratory nuclear magnetic resonance spectrometer (6-23 T).

After preliminary experiments, two different ratios of [$FeCl_3.6H_2O$:$FeSO_4.1.5H_2O$] (*w/w*) – (1:2) MP1 and (3:1) MP2 – were tested in the production of MAC due to rapid and efficient separation from solution by a magnet verified for the MP synthesised in both conditions.

2.2 | Production of magnetic activated carbon

During the *in-situ* synthesis route, WPAC was added to the iron salt solution prior to the addition of base and the coprecipitation reaction took place as described previously, followed by the washing, drying and grinding steps. The mass of WPAC added was defined in relation to the total mass of iron salts in solution. WPAC/Fe salt proportions of 1:2, 1:3, 1:4 and 1:6 (*w/w*) were tested (Table 4). The *ex-situ* route involved the suspension of both WPAC and MP in deoxygenized water, under nitrogen flux, and subsequent pH adjustment to a pH value in between the PZC of both materials in suspension, thus promoting surface attraction. The PZC of the precursor WPAC is pH ~5 (25 ºC) [69] whereas the PZC of magnetite, the most magnetic iron oxide, is pH ~ 6.4-8.0 (20-25 ºC) [103]. Accordingly, the pH of the suspension was kept between the pH interval 5-6 for 1 h, under agitation and nitrogen flux, thus assuring a prevalence of opposing average surface charges for WPAC (negative) and magnetic iron oxide (positive). The resulting materials were magnetically decanted, dried at 40 ºC and grinded into a powder.

Table 4 – MAC production nomenclature and process routes

***in-situ* route**			
Material nomenclature	WPAC:Fe salt (w/w)	WPAC % (w/w)	$FeCl_3.6H_2O$:$FeSO_4.1.5H_2O$ (w/w)
MAC2-MP1	(1:2)	33	(1:2)
MAC3-MP1	(1:3)	25	(1:2)
MAC4-MP1	(1:4)	20	(1:2)
MAC6-MP1	(1:6)	14	(1:2)
MAC3-MP2	(1:3)	25	(3:1)
MAC4-MP2	(1:4)	20	(3:1)
MCAC2-MP1*	(1:2)	33	(1:2)
***ex-situ* route**			
Material nomenclature	WPAC:MP (*w/w*)	WPAC % (*w/w*)	$FeCl_3.6H_2O$:$FeSO_4.1.5H_2O$ (*w/w*)
MACX1-MP1	(1:1)	50	(1:2)

*commercial PAC (PBFG4 – Chemviron) used as precursor, for comparison purposes

3 | Physical and chemical characterization of magnetic activated carbons

3.1 | Total organic carbon

Total organic carbon was determined, for selected samples, by calculating the difference between total carbon (TC) content and inorganic carbon (IC) content, both determined with a TOC analyser (Shimadzu, TOC-VCPH solid sample module SSM-5000A, Japan). Glucose ($C_6H_{12}O_6$, 40% of carbon) and sodium carbonate (Na_2CO_3, 11% of carbon) were used as standards to evaluate the calibration of the equipment for TC and IC determination, respectively. For TC determination 30 mg of sample were weighed in small porcelain crucibles and then analysed. For IC determination, the same sample mass was used, digested with phosphoric acid (H_3PO_4, 50%) and subsequently analysed. Samples were analysed in three replicates and the carbon content was obtained by the average of such measurements.

3.2 | Fourier transform infrared spectroscopy with attenuated total reflectance

Fourier transform infrared spectroscopy with attenuated total reflectance spectra were obtained using a FTIR spectrophotometer (Shimadzu, IRaffinity-1, Japan), using an attenuated total reflectance (ATR) module, with a nitrogen purge. The measurements were recorded in the range of 700-4000 cm^{-1}, 4.0 cm^{-1} resolution, 128 scans and with atmosphere and background correction. PS, WPAC and all MAC and MP were analysed.

3.3 | Specific surface area and pore morphology

Physical textural properties were accessed in a surface area and porosity analyser (Micromeritics, Gemini VII 2380, USA) by nitrogen adsorption isotherm at -196 ºC, after sample degasification overnight at 120 ºC. The following parameters were determined: S_{BET} was calculated by the Brunauer-Emmett-Teller (BET) equation [48] in the relative pressure range 0.01-0.1; total micropore volume (W_0) was determined by the Dubinin-Radushkevich equation [49]; total pore volume (V_p) was estimated from the amount of

nitrogen adsorbed at a relative pressure of 0.99; average pore width (D) was calculated as $D = 2.V_p/S_{\mathrm{BET}}$ [77]. The produced WPAC, MP1 and all MAC derived from MP1 were analysed.

3.4 | Scanning electron microscopy

Superficial morphology was analysed through SEM images obtained using a scanning electron microscope (Hitachi, S4100, Japan) at magnifications of 100x, 500x, 3000x, 10000x and 50000x. WPAC, MP1 and all MAC derived from MP1 were analysed.

3.5 | Point of zero charge

Point of zero charge was determined by the pH drift method, similarly to Jaria et al. (2015) [79] for the two selected best materials (MAC4-MP1 and MACX1-MP1). A set of ten different pH solutions (pH_i = 2-11) of 0.1 M NaCl (99,5%, José Manuel Gomes dos Santos, Portugal) were prepared, and initial pH (pH_i) values were adjusted with 0.1 M and 0.01 M HCl (37%, Fluka), and 0.1 and 0.01 M NaOH (AzkoNobel, Netherlands). 1 mg of selected samples was incubated in 40 mL of each pH solution (25 mg L^{-1}), in propylene tubes for 24 h at 25 ºC, in an overhead shaker. The final pH (pH_f) was measured and PZC was determined by plotting ΔpH (pH_f – pH_i) *versus* pH_i. The PZC is the pH value corresponding to the x-axis interception of the obtained curve.

3.6 | Vibrating sample magnetometer

The magnetization measurements for all MAC and MP samples were carried out using a vibrating sample magnetometer (Quantum Design, MPMS®3, USA) with an applied magnetic field of about 13 kOe, at 5 torr and 290-310 K in a helium rich atmosphere. Sample saturation magnetization was determined by plotting magnetic moment *versus* applied magnetic field, the saturation magnetization corresponded to the *plateau* value of magnetic moment reached divided by the sample mass (1 mg). WPAC, MP1 and MP2 particles, all MAC derived from MP1 and MAC4-MP2 were analysed.

3.7 | X-ray diffraction

X-ray diffraction analysis was performed to evaluate the presence of magnetic iron oxides in the produced materials. Measurements were performed at room temperature with a PANalytical Empyrean powder diffractometer using monochromated CuKα radiation (λ = 1.541º A) in the 10-80º 2θ range at 0.02º resolution, and 4000 acquisition points per step. The incident beam optics included a Soller slit of 0.04 rad, a 10 mm fixed mask, a divergence fixed slit of 1=4 and an anti-scatter slit of 1=8. The diffracted beam optics included a Soller slit of 0.04 rad and anti-scatter slit of 7.5 mm. The two best MAC (MAC4-MP1 and MACX1-MP1), WPAC and MP1 were analysed.

4 | Analytical method – capillary electrophoresis

Adsorptive performance of the produced materials was evaluated by determining adsorbate concentration remaining in solution after adsorption and subsequently the adsorption capacity. CE was used as main analytical method for this purpose. The analysis mode was based entirely on a MEKC separation method operated in a dynamically coated fused silica capillary as described in Calisto (2011) [101]. Analyses were performed in a Beckman P/ACE MDQ (Fullerton, CA, USA) equipped with a photodiode array UV-Vis detector, using the software 32 Karat. The fused silica capillary had a total length of 40 cm (30 cm to the detection window) and 75 μm of internal diameter.

Additionally, in the first preliminary adsorption tests, CBZ was also quantified by UV-Vis spectrophotometry due to the simplicity and quickness of the method which allowed to determine the relevant synthesis conditions and progress with the work.

4.1 | Capillary coating

Briefly, the coating procedure consisted of strong deprotonation of the capillary wall silanol groups with NaOH 1 M (30 min), followed by rinsing with ultrapure water (15 min). The negatively charged surface was then coated with polybrene (hexadimethrine bromide) 0.5% (*w/v*) in NaCl 0.5 M (20 min), followed by another ultrapure water rinsing period (2 min). The positively charged surface was flushed with running buffer (20 min) – 15 mM sodium borate (electrolyte) + 20 mM SDS (anionic surfactant) – which coated the capillary wall with its final negatively charged surface.

The capillary was subjected to a daily washing routine starting with running buffer (20 min) in the beginning of the day and ultrapure water (5 min) at the end of the day. Both extremities of the capillary were kept submerged in ultrapure water when not in use.

4.2 | Sample preparation and separation procedure

The use of an internal standard in every sample was required, considering that sample injection was made by pressure and it is not possible to assure constant sample volume injection in CE. CBZ quantification was established by the mean peak area ratio of analyte and internal standard, relying on a constant proportion of sample and internal standard injected each time. Ethylvanillin was used as internal standard and a 167 mg L^{-1} stock solution (diluted in ~10% of acetonitrile and completing the volume with ultrapure water) was prepared and stored at 4 ºC in the dark. A 10% dilution in ultrapure water was used for sample preparation, made fresh every day and stored under the same conditions.

A 15 mM sodium borate and 20 mM SDS in ultrapure water solution was used as running buffer, prepared fresh every two days and stored at 4 ºC. A 100 mM sodium borate solution in ultrapure water was used as electrolyte and added to each sample along with internal standard. All samples and buffer solutions were filtered through a 0.22 µm Whatman PVDF Membrane Filter prior to analysis.

Samples were prepared in CE vials by adding 1350 µL of sample, 150 µL of 100 mM sodium borate solution and 30 µL of ethylvanillin 10% to each sample vial.

Analysis were made with an applied potential of 25 kV and a capillary temperature of 25 ºC. CBZ detection was performed at wavelength 214 nm.

Each sample vial was analysed three times by the instrument. Separation procedure was as follows:

1| H_2O rinse (1 min at 20 psi)
2| Running buffer rinse (2 min at 20 psi)
3| Sample injection (4 s at 0.5 psi)
4| H_2O injection (3 s at 0.5 psi)
5| Separation with running buffer (3-5 min)

4.3 | Calibration curve

The standardization of the instrument signal was performed by means of a series of samples of known CBZ concentration, using a calibration curve with seven standard solutions prepared by dilution of a 5 mg L^{-1} CBZ solution: 0.25, 0.50, 1.0, 2.0, 3.0, 4.0 and 5.0 mg L^{-1}. The calibration curve was fitted by the least-squares linear regression method, given by the Equation (10):

$$y = a + bx \tag{10}$$

where y is the ratio between the CBZ peak area of the sample and the peak area of the internal standard, x is the concentration of the analyte, a is the intercept on the y-axis and b is the slope of the curve [104]. Every standard solution was prepared as described in section II-4.2 and analysed in quadruplicate by the instrument.

Limit of detection (LOD) and limit of quantification (LOQ) were determined according to Equations (11) and (12), respectively:

$$LOD = a + 3S_a \tag{11}$$

$$LOQ = a + 10S_a \tag{12}$$

$$S_a = S_{y/x}\sqrt{\frac{\sum_i x_i^2}{n\sum_i (x_i - \bar{x})^2}} \tag{13}$$

where S_a is the error associated with y-intercept of the curve (a), estimated by the standard deviation in the y-direction ($S_{y/x}$) and calculated by Equation (13).

5 | Batch adsorption studies

Adsorptive performance of the produced materials was evaluated by batch adsorption tests. The anti-epileptic drug CBZ was used as analyte in both ultrapure water and real WWTP effluent matrix, at initial concentration of 5 mg L^{-1}. Final treated effluent was gathered at a local urban WWTP (Aveiro, Portugal) that receives an average wastewater flow of 39 278 m^3 per day, which is subjected to primary followed by biological treatment. The effluent was vacuum filtered through a 0.45 μm Supor-450 Cellulose Membrane Disc Filter, immediately after collection. After filtration to remove suspended organic matter and solid residues, the effluent was stored at 4 ºC in the dark, for a

maximum period of three weeks. WWTP effluent pH (Hanna Instruments, HI2020-02 pH meter), conductivity (WTW meter) and dissolved organic carbon (DOC) (Shimadzu, TOC-VCPH liquid sample module SSM-5000A, Japan) were measured.

Materials' dosage was weighed in a microbalance, with an uncertainty of ± 0.001 mg, into propylene tubes with 40 mL of 5 mg L^{-1} CBZ solution and shaken at 80 rpm in an overhead shaker at 25 ºC. All experiments were replicated three times and CBZ solution incubated without adsorbent was used as control. After the incubation period, all samples were filtrated through a 0.22 μm Whatman PVDF Membrane Filter, to separate the adsorbent from the aqueous phase, and CBZ was quantified by capillary electrophoresis, according to the procedure described in section II-4.

5.1 | Preliminary adsorption tests

Preliminary adsorption experiments were carried out to evaluate which of the produced materials had better adsorptive performance for CBZ in ultrapure water. These tests were performed in simultaneous with the synthesis of MAC described in section II-2.2. Specific adsorbent concentrations were tested (Table 5) for an incubation period of 24 h. The results provided information that assisted not only in the final selection of the two best magnetic materials to be fully characterized and evaluated, but also in the setting of synthesis parameters for the preparation of MAC.

Table 5 – Dose of material and analytical method used in preliminary CBZ adsorption experiments in ultrapure water

Material	Material dosage (mg L^{-1})	Analytical method
WPAC	25; 50	CE, UV-Vis
MAC2-MP1	50	CE, UV-Vis
MAC3-MP1	50	UV-Vis
MAC4-MP1	25; 50	UV-Vis
MAC4-MP2	50	UV-Vis
MAC6-MP1	25; 50; 75	CE, UV-Vis
MACX1-MP1	25; 50	UV-Vis
MP1	25; 50	CE, UV-Vis
MCAC2-MP1	50	UV-Vis

CE – capillary electrophoresis
UV-Vis – ultraviolet-visible spectrophotometry

5.2 | Kinetic adsorption study

The two selected best MAC (MAC4-MP1 and MACX1-MP1) were subjected to a kinetic adsorption study to determine adsorption equilibrium time. The kinetic study involved the incubation of a fixed concentration of material for different periods of time. In that sense and based on preliminary experiments, 25 mg L^{-1} was established as the fixed concentration for all MAC, in both ultrapure water and real effluent. Accordingly, 40 mL of a 5 mg L^{-1} CBZ solution was incubated with the referred fixed amount of MAC for 5, 10, 15, 30, 60 and 120 minutes in ultrapure water and 5, 10, 15, 30, 60, 120 and 240 minutes in real effluent.

The amount of CBZ adsorbed at each time (q_t (mg g^{-1})) was determined by Equation (1) and kinetic parameters were determined using the pseudo-first and pseudo-second order models (Equations (6) and (8), respectively). Experimental data model fitting was performed by the non-linear regression method, using Graph Pad Prism 5 software, and MatLab 7.0 software was used for peak integration.

5.3 | Equilibrium adsorption study

Considering the adsorption equilibrium period determined during the kinetic studies, equilibrium adsorption experiments were performed to determine maximum adsorption capacities (q_m (mg g^{-1})) for the two best materials. A range of different adsorbent concentrations were tested in ultrapure water (10-60 mg L^{-1} for MACX1-MP1 and 10-55 mg L^{-1} for MAC4-MP1) and real effluent (10-80 mg L^{-1} for MACX1-MP1 and MAC4-MP1) for both materials. The materials were incubated for 2 h in ultrapure water and 4 h in effluent, as these periods ensured the attainment of equilibrium.

Similarly to the kinetic studies, the quantity of adsorbed CBZ at equilibrium (q_e (mg g^{-1})) for each adsorbent concentration was determined using Equation (1). Langmuir and Freundlich non-linear equilibrium models (Equations (2) and (4), respectively) were used to fit the experimental data in order to determine equilibrium parameters using Graph Pad Prism 5. MatLab 7.0 software was used for peak integration.

5.4 | Evaluation of pH and matrix interference

To evaluate the influence of pH in the adsorption process a set of adsorption experiments were carried out in 0.01 M phosphate buffer at the effluent pH (~8.0). A 0.1 M phosphate buffer solution was prepared from 1 M stock solutions of K_2HPO_4 and KH_2PO_4 and subsequently diluted to the desired 0.01 M concentration. A 5 mg L^{-1} CBZ solution was prepared using the referred buffer and the solution pH adjusted to 8.0 with 0.1 M H_3PO_4 and 0.1 M NaOH. A fixed concentration of 25 mg L^{-1} was used for both selected MAC and for WPAC, and 40 mL of buffered CBZ solution was used in each tube. Experiments were run in triplicate and incubation period was 2 h, assuring both systems reached adsorption equilibrium. Buffered CBZ solution incubated under the same conditions was used as control.

The amount of adsorbed CBZ at equilibrium (q_e (mg g^{-1})) for each material was determined using Equation (1). MatLab 7.0 software was used for peak integration.

5.3 | Equilibrium isotherm and kinetic model fitting error evaluation

In order to evaluate the adequacy of the model fitting, three parameters were used to choose the best fitting model for the equilibrium and kinetic studies. All parameters were provided by the Graph Pad Prism 5 software.

The parameters were the coefficient of determination (R^2), the standard deviation of residuals ($S_{x/y}$) and the absolute sum-of-squares (ASS), given by the following equations:

$$R^2 = \frac{1 - SS_{regression}}{SS_{total}} \tag{14}$$

where $SS_{regression}$ refers to the sum-of-squares of the regression and SS_{total} is the total sum-of-squares,

$$S_{y/x} = \sqrt{\frac{\sum(residual^2)}{n - K}} \tag{15}$$

where the residual is the vertical distance (in y units) of the experimental point from the fit curve, n is the number of data points and K is the number of parameters fitted by the regression,

$$ASS = \sum (y_i - \hat{y})^2 \quad (16)$$

where $(y_i - \hat{y})$ is the vertical distance between the data point (y_i) and the regression curve $(\hat{y})$.

The lowest value of ASS and $S_{y/x}$ indicates the best model and maximizing the R^2 value denotes greater agreement between the experimental data and the model prediction.

III. Results and Discussion

1 | Characterization of magnetic adsorbents

The production yield of the precursor WPAC was calculated (Equation (9)) and determined to be 5.9%. Such value is coherent with previous works [69] and can be explained by the KOH chemical activation and the HCl washing step. The chemical activation is the main responsible for the formation of porosity which yields a very low-density and microporous AC. The HCl washing step, especially through inorganic matter removal, represented about 96 % of weight loss after pyrolysis.

1.1 | Total organic carbon

The results of total organic carbon analysis are presented in Table 6. It is possible to conclude that pyrolysis strongly contributes to the increase in organic carbon content, proved by the 40% increment when comparing WPAC to PS. Inorganic carbon content is residual for WPAC which reflects its efficient removal during HCl washing steps.

Table 6 - TOC analysis for WPAC and derived magnetic adsorbents

Material	TC (%)	IC (%)	OC (%)
	Mean ± SD	Mean ± SD	Mean ± SD
PS	33.1 ± 0.1	4.6 ± 0.4	28.5 ± 0.4
WPAC	68.2 ± 0.4	0.11 ± 0.04	68.1 ± 0.3
MAC2-MP1	35.0 ± 0.5	0.031 ± 0.002	34.9 ± 0.5
MAC3-MP1	29.1 ± 0.2	0.11 ± 0.02	28.9 ± 0.2
MAC4-MP1	25.2 ± 0.1	0.12 ± 0.02	25.0 ± 0.1
MAC4-MP2	27.8 ± 0.1	0.11 ± 0.01	27.7 ± 0.1
MAC6-MP1	19.9 ± 0.1	0.045 ± 0.007	19.8 ± 0.1
MACX1-MP1	33.9 ± 0.2	0.07 ± 0.05	33.9 ± 0.3
MP1	0.154 ± 0.005	0.19 ± 0.02	< LOD
MP2	0.56 ± 0.05	0.11 ± 0.04	< LOD
MCAC2-MP1	42.4 ± 0.8	0.090 ± 0.002	42.3 ± 0.8
PBFG4*	74.8 ± 0.7	0.07 ± 0.05	75 ± 1

TC – total carbon; IC – inorganic carbon; TOC – total organic carbon
*Results from Calisto et al. (2014) [77]

The results also highlight a decrease in organic carbon for all MAC in comparison to WPAC. This is due to the introduction of magnetic iron oxide particles (MP) into the structure of WPAC, inevitably reducing the relative organic carbon content since such particles have no contribution in organic carbon content (Table 6). Besides, this effect is proportional to the WPAC/Fe salt ratio. For instance, organic carbon content plummeted from 68.1% in WPAC to 19.8% in MAC6-MP1 (1:6 ratio), whereas a less accentuated decrease was observed for MAC2-MP1 (34.9%) (1:2 ratio).

1.2 | Specific surface area and pore morphology

Table 7 lists several important textural parameters that were determined for the produced materials. The WPAC, used as precursor for MAC synthesis, presents a S_{BET} value consistent with previous works [69,105] and in line with characteristic values for PAC. In fact, WPAC has a S_{BET} much higher than the one of PBFG4, a commercial PAC used for comparison purposes. From these results, it is possible to infer the highly microporous structure of WPAC as the micropore volume (W_0) accounts for approximately 58% of total pore volume (V_p).

The results also suggest that S_{BET} and V_p are negatively affected by the presence of magnetic iron oxides in the MAC. However, the D values for MAC are compatible with a microporous material (< 2 nm). Magnetic particles MP1 have a relatively low S_{BET}, V_p and W_0, hence its presence in the magnetic composite causes an inevitable decrease in the referred parameters. Additionally, due to the nanometric size of the MP produced through coprecipitation [85], their possible deposition on WPAC's complex micropore structure ultimately represents a significant reduction in micropore volume which is accentuated by an increased proportion of iron salt in relation to AC, and therefore an increased proportion of MP.

For the *ex-situ* MACX1-MP1, the reduction of S_{BET} and W_0 is of the same magnitude as the reduction of the WPAC proportion, approximately 50%. However, this linear relation is not so clear for the *in-situ* MAC since the iron salt content does not directly translate into MP content. This can possibly be explained by the interference of the AC in the coprecipitation process which might influence MP synthesis, size and shape, possibly reducing the final MP content in the magnetic adsorbent.

Comparing with a commercial non-magnetic PAC (PBFG4), MAC2-MP1 and MACX1-MP1 have similar physical properties in terms of S_{BET} and W_0 with the advantage of being effectively retrievable from solution *via* magnetic separation.

Table 7 – Specific surface area and pore morphology of the produced materials and a commercial PAC (PBFG4, Chemviron)

Material	S_{BET} ($m^2\ g^{-1}$)	V_p ($cm^3\ g^{-1}$)	W_0 ($cm^3\ g^{-1}$)	D (nm)
WPAC	1533	1.06	0.61	1.39
MAC2-MP1	805	0.77	0.32	1.32
MAC3-MP1	652	0.60	0.26	1.85
MAC4-MP1	551	0.60	0.22	2.17
MAC6-MP1	449	0.44	0.18	1.97
MACX1-MP1	777	0.62	0.31	1.58
MP1	23	0.16	0.01	13.59
PBFG4*	848	0.36	0.30	0.84

S_{BET} – Specific surface area; V_p – Total pore volume; W_0 – Micropore volume; D – Average pore diameter
*Results from Calisto et al. (2014) [77]

1.3 | Scanning electron microscopy analysis

Scanning electron microscopy analysis was performed to evaluate textural properties and outer surface morphology of the adsorbents. Figures 9 and 10 exhibit SEM images from both WPAC and MP1, as well as from *in-situ* MAC and *ex*-situ MAC.

In Figure 9 a), it is clear the complex porous structure of the WPAC and in Figure 9 b) (50000x) it is possible to observe the nanometric size of the MP1 particles. From the analysis of MAC and WPAC images at amplifications of 10000x or 50000x, it is obvious that MAC surfaces are rougher than the precursor WPAC. This roughness is associated with the deposition of magnetic particles throughout the surface of the AC. Figure 10 a) (50000x) is the one that better demonstrates this phenomenon which might explain the verified pore volume reduction or even pore blockage. Analysing the *in-situ* MAC images, it becomes clear that increasingly iron salt proportions correspond to rougher surfaces and increasingly pore constraints. This analysis can be corroborated with the results from Table 7, which indicate S_{BET} reduction.

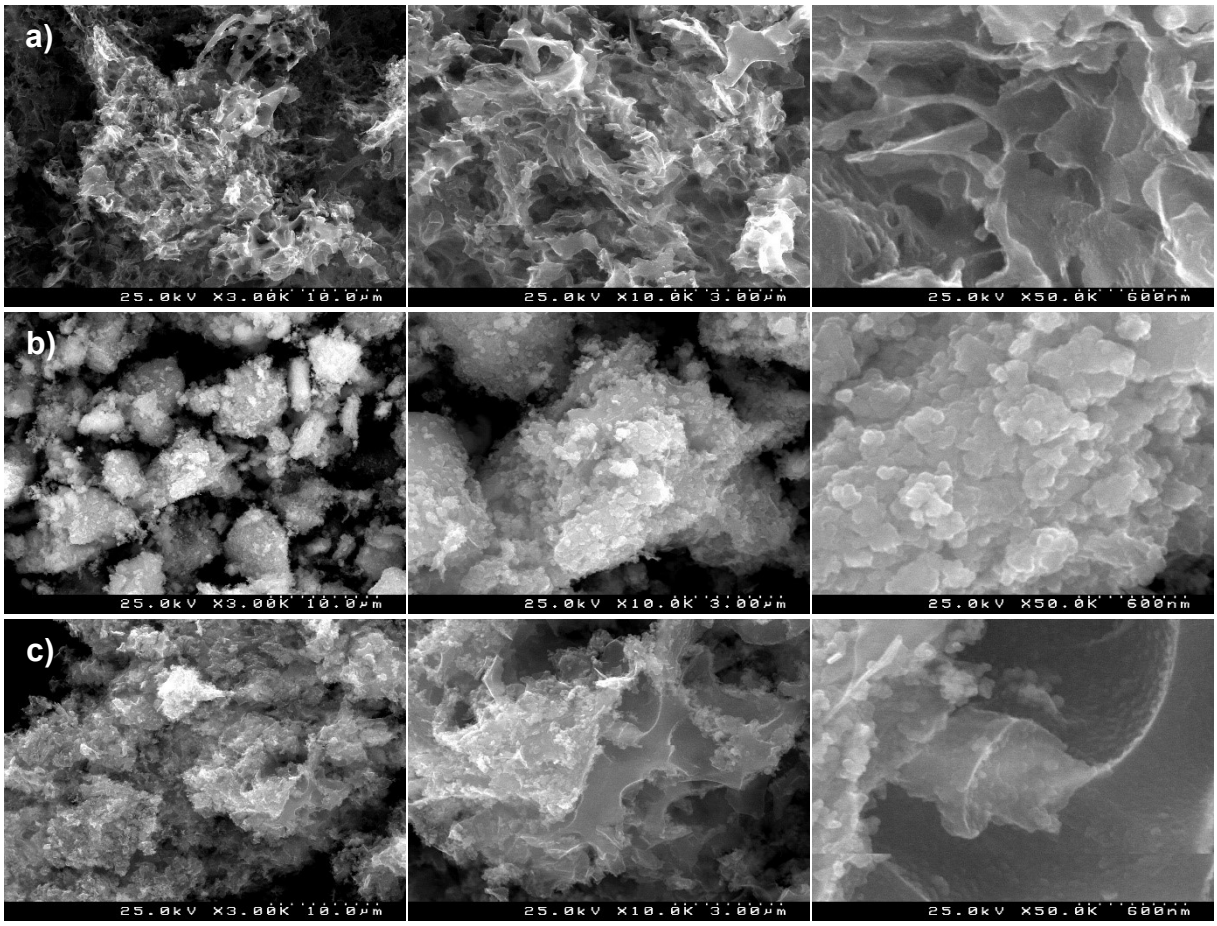

Figure 9 – SEM images of a) WPAC; b) MP1; c) MAC2-MP1 at magnifications of 3000x, 10000x and 50000x (left to right)

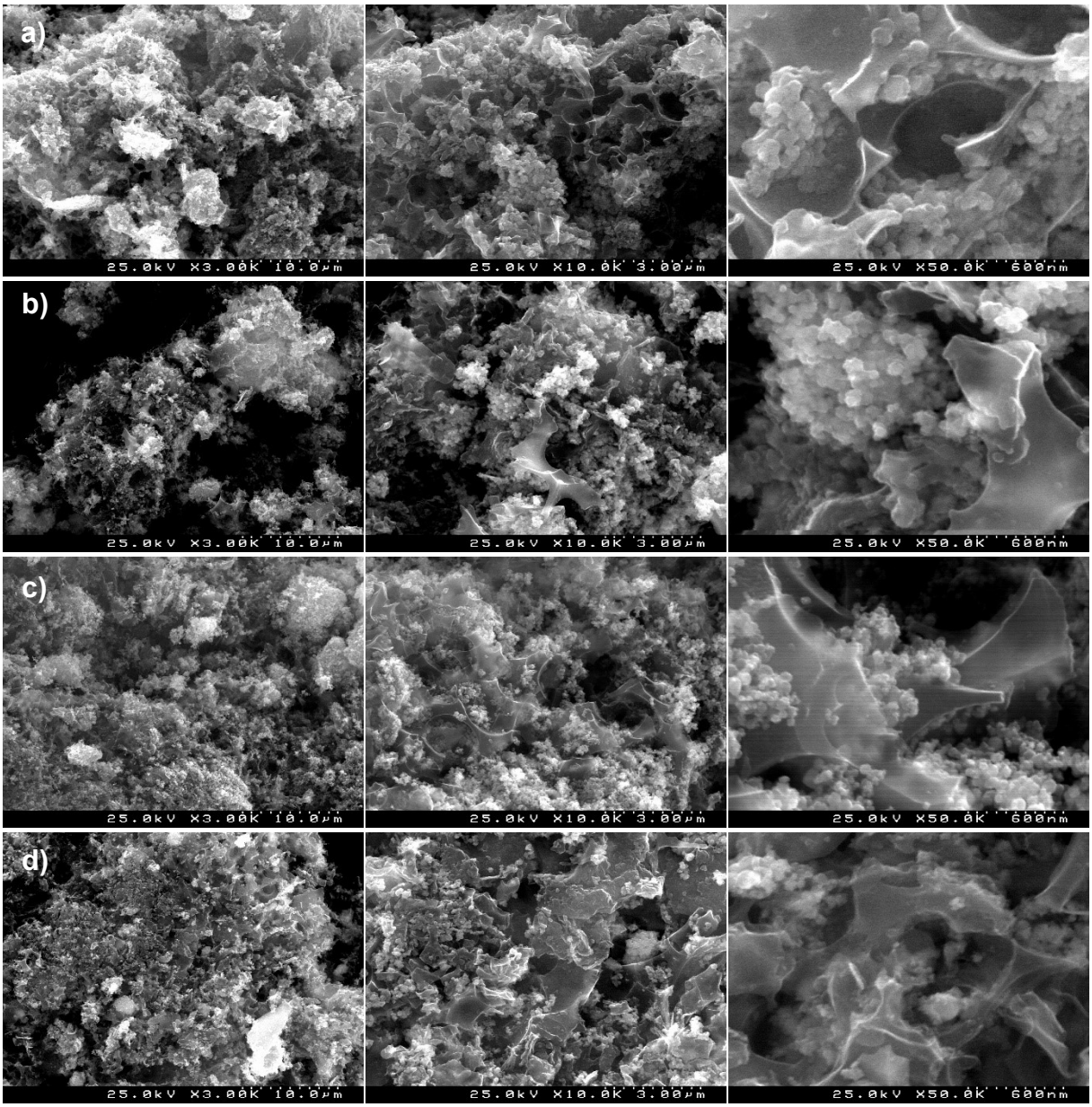

Figure 10 – SEM images of a) MAC3-MP1; b) MAC4-MP1; c) MAC6-MP1; d) MACX1-MP1 at magnifications of 3000x, 10000x and 50000x (left to right)

The images from MACX1-MP1 show that no visible distinction can be made between *in-situ* and *ex-situ* MAC, in what concerns the deposition of MP on their surfaces. Similar images are found in the literature for MAC produced in an identical manner as *in-situ* [97] and *ex-situ* [96].

1.4 | Vibrating Sample Magnetometer analysis

The results from VSM analysis are depicted in Table 8. As expected WPAC's magnetic properties are neglectable, thus any contribution to the increment of saturation magnetization value is related to the loading of magnetic iron oxides onto its surface.

Considering *in-situ* MAC samples, an increase in the initial weight proportion of iron salts is directly associated with an increase in saturation magnetization. However, the assumption of a linear increase in saturation magnetization with relation to the proportion of iron salt cannot be made. The *ex-situ* MACX1-MP1 weight content is composed by 50% of WPAC, nonetheless its saturation magnetization value is approximately 77% of the MP1 particles.

Table 8 – Saturation magnetization values for the produced adsorbents and MP

Material	Saturation magnetization (emu g^{-1})
WPAC	0.28
MAC2-MP1	30.56
MAC3-MP1	44.63
MAC4-MP1	51.46
MAC4-MP2	10.90
MAC6-MP1	76.13
MACX1-MP1	43.33
MP1	56.16
MP2	100.73

Two different iron salt ratios where tested for the synthesis of MP. MP2 particles are almost twice more magnetic than MP1, indicating that the (3:1) [$FeCl_3.6H_2O$:$FeSO_4.1.5H_2O$] mass ratio (in relation to the MP1 (1:2) ratio) favours the synthesis of magnetic iron oxides, such as magnetite, to the detriment of non-magnetic ones, such as hematite or goethite. In fact, the referred ratio is commonly found in the literature as a standard ratio for the production of magnetite [85]. However, during preliminary tests to access the MAC synthesis conditions and considering visual responsiveness to a neodymium magnet, magnetic separation was achieved more successfully when using the MP1 ratio. This was quantitively corroborated with the VSM results (Table 8). When MP2 ratio was applied to the *in-situ* MAC production route

(MAC4-MP2 – 10.90 emu g^{-1}), the VSM analysis revealed lower magnetic properties when compared to the analogous MP1 magnetic adsorbent (MAC4-MP1 – 51.46 emu g^{-1}). As for MAC3-MP2 (Table 4), magnetic separation from solution was unachieved and the material was not subject of VSM analysis.

It is important to refer that all *in-situ* and *ex-situ* MAC presented in Table 8 are magnetically responsive to a permanent magnet. Still, a rapid or immediate and effective separation from solution could only be achieved for MAC6-MP1, MAC4-MP1, MAC3-MP1 and MACX1-MP1.

1.5 | Fourier transform infrared spectroscopy with attenuated total reflectance analysis

In this study, the FTIR-ATR analysis allowed for a qualitative evaluation of the composition of the produced materials, providing insightful information about their surface chemistry which strongly influences adsorption. Figure 11 presents the spectra of WPAC and its precursor PS, indicating the main vibrational bands and evidencing the differences in FTIR-ATR spectra before and after pyrolysis.

Several chemical bonds within the analysed structure selectively absorb infrared radiation, which enables the establishment of correlations between peaks in the FTIR-ATR spectra and the surface chemistry composition. The peak at around 1650 cm^{-1} is often associated with aromatic C=C stretching and vibration [45] and the peaks in the region of 700-750 cm^{-1} can be assigned to in-plane and out-plane deformation vibrations of aromatic rings and C-C stretching [106], as well as aromatic C-H bending at around 1320 cm^{-1}. A broad band (3000-3700 cm^{-1}) peaking at 3330 cm^{-1}, in addition to peaks at around 2930 cm^{-1}, can be attributed to alcohol or phenolic groups C-O stretching or bending vibrations [45,106]. Aliphatic C-H stretching signals can also be deduced from the band around 2815-3000 cm^{-1} [106]. Visible peaks at 1030, 1110 and 1160 cm^{-1} can be related to C-O-C stretching vibrations. Specific identity peaks around 1430 cm^{-1} and 870 cm^{-1} are indicators of the presence of carbonate groups. The infrared absorbance pattern presented in Figure 11 is compatible with the cellulosic composition of the precursor PS. A decrease in peak intensity and complexity of the spectra can be noticeably observe following pyrolysis.

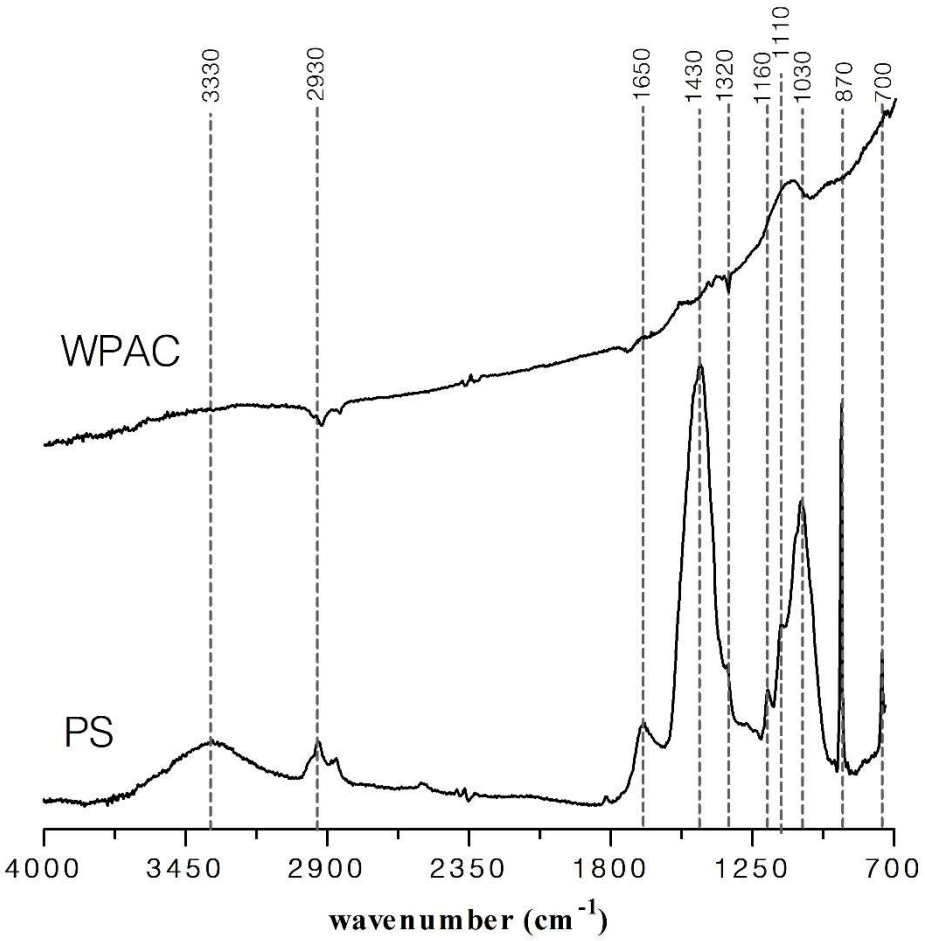

Figure 11 – FTIR-ATR spectra (absorbance *vs* wavenumber) of PS and WPAC

The WPAC spectrum indicates mainly the presence of aromatic groups, ether groups (broad peak at 1030-1160 cm^{-1}) and other oxygen containing functional groups such as alcohol, carboxylic, lactone or phenol groups, which is consistent with typical surface chemistry of AC derived from a cellulosic precursor. Previous studies suggest the presence of predominantly phenol and lactone groups on the surface of WPAC [69], as determined by Boehm's titrations. Noticeably, the characteristic peak of carbonate groups is absent in the WPAC spectrum, which might be explained by the effective removal of inorganic fraction during the HCl washing step and is, therefore, coherent with the TOC results (Table 6).

The characteristic bands for magnetic iron oxides, namely magnetite and maghemite, are associated with Fe-O bonds and are typically located at wavenumber below 700 cm^{-1}. For instance, magnetite spectrum has distinctive broad bands at around 580 and 400 cm^{-1}, whereas maghemite has characteristic peaks in the interval between 640 cm^{-1} and 305

cm^{-1} [83]. At this wavenumber range, magnetic iron oxide identification in MAC samples was hampered by FTIR-ATR spectrum noise and no valid information was deduced from the analysis.

1.6 | Point of zero charge determination

In order to predict possible electrostatic interactions between adsorbate and adsorbent, it is crucial to determine the PZC to estimate the surface net charge of the materials at a specific pH. Figure 12 presents the ΔpH *vs* pH_i plots used in the PZC determination for the selected best materials MAC4-MP1 and MACX1-MP1. The PZC corresponds to the pH value where ΔpH=0, which means that the pH of the solution is similar to that of the surface of the adsorbent.

For MAC4-MP1 and MACX1-MP1 the determined PZC values were 6.0 and 5.7, respectively. This means that at pH 6.0 and 5.7 the material's net surface charge is zero.

In aqueous systems, iron oxides tend to adsorb water or hydroxyl groups which in turn can coordinate with more than one iron atoms. The two magnetic iron oxides, magnetite and maghemite have PZC in the range of 6.4-8.0 and 5.5-7.5 [103], respectively, whereas WPAC has a slighly more acidic PZC (~5) [69]. The contribution of MP deposited on the surface of WPAC can explain the slight increase in PZC for both magnetic materials analysed.

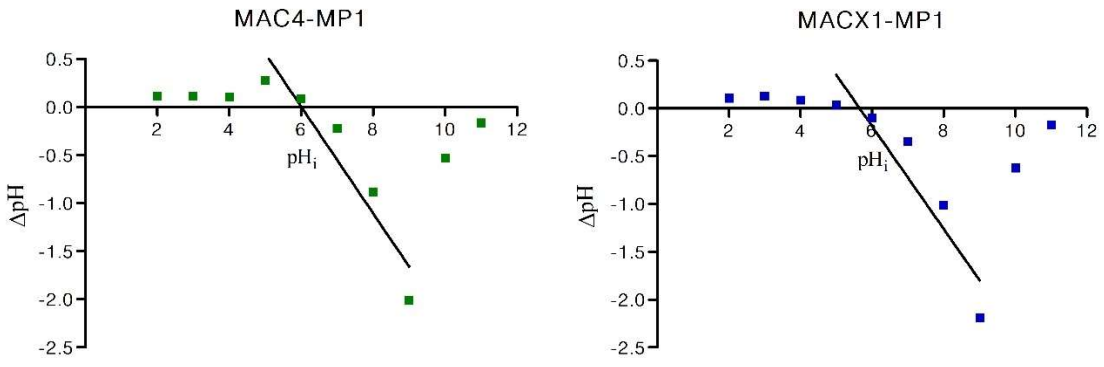

Figure 12 – PZC determination plots for MC4-MP1 and MACX1-MP1

1.7 | X-ray diffraction analysis

X-ray diffraction patterns for WPAC, MP1, *in-situ* MAC4-MP1 and *ex-situ* MACX1-MP1 are represented in Figure 13. AC are characterized by their amorphous structure composed by non-graphitic and non-graphitizable carbon, without any measurable crystallographic order. However, some intermediate structures between graphite and amorphous state (turbostratic structures) can be deduced from the XRD pattern of WPAC (28.2º and 47.5º) [107]. Additionally, peaks at around 33.0º and 56.4º can be associated with potassium compounds, due to KOH activation, and some oxygen functional groups, respectively [108].

A common characteristic XRD pattern (30.2º, 35.4º, 43.2º, 53.5º, 57.1º and 62.8º) can be observed for MP1, MAC4-MP1 and MACX1-MP1 materials, which is associated with the cubic crystal structure of magnetite and maghemite [83]. The distinction between the two magnetic iron oxide is not possible by XRD but it is possible to state that magnetite and maghemite are the two main crystalline components present in the *ex-situ* and *in-situ* MAC.

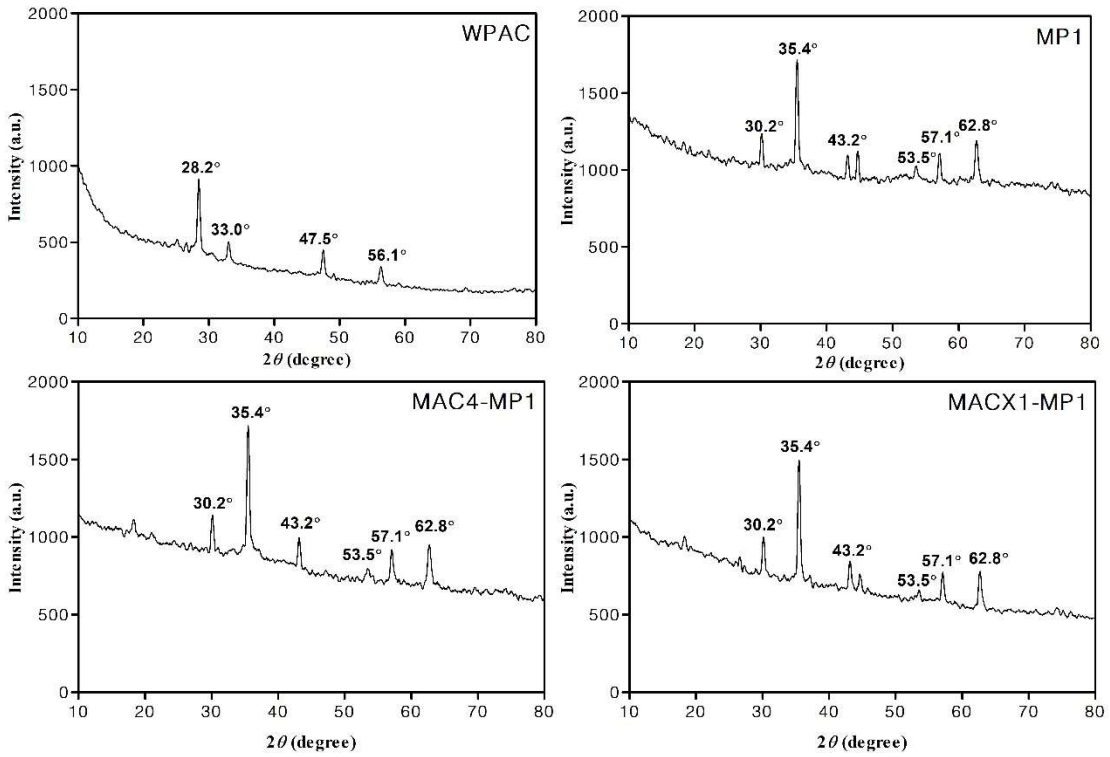

Figure 13 – XRD patterns of WPAC, MP1, MAC4-MP1 and MACX1-MP1

2 | Adsorption kinetic and equilibrium studies

As previously described, kinetic and equilibrium studies were performed for the two best MAC in both ultrapure water and real effluent collected from a local WWTP. The pH, conductivity and DOC measurements for the effluent are listed in Table 9.

Table 9 – WWTP effluent pH, conductivity and DOC analysis results

Sample	pH	Conductivity (mS cm^{-1})	DOC (mg L^{-1}) Mean ± SD
Effluent	8.07	2.77	19.4 ± 0.3

The results are coherent with previous effluent collections from the same WWTP [105]. In Silva et al. (2019) [105], WPAC (S_{BET} of 1627 m^2 g^{-1}) single-component kinetic and equilibrium isotherm studies were performed for three pharmaceuticals, including CBZ, in ultrapure water and WWTP effluent. The results of those studies will be used as comparison in this work, given the similarity of WPAC properties and effluent characteristics in both works.

2.1 | Calibration of the analytical method

Quantification of CBZ in solution was performed by CE. For every capillary used, a calibration curve was developed according to the description in section II-4.3. Figure 14 provides an example of one of the CBZ calibration curves obtained and Table 10 lists the determined linear regression parameters.

Table 10 – CBZ calibration linear regression parameters

Parameter	
a y-intercept	0.06 ± 0.01
b (slope)	0.63 ± 0.01
R^2	0.9971
$S_{y/x}$	0.0431

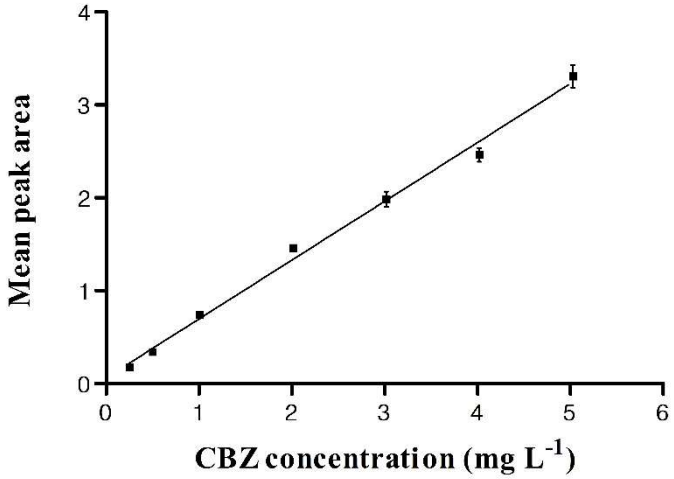

Figure 14 – Example of a calibration curve used for CBZ concentration determination

The LOD and LOQ for this particular case was 0.09 mg L^{-1} and 0.16 mg L^{-1}, respectively.

2.2 | Preliminary adsorption tests

Preliminary adsorption tests were performed in ultrapure water, for 24 h, and the obtained results are summarized in Table 11. The best materials were selected for further extensive adsorption studies. As previously stated, along with an inevitable decrease in S_{BET}, a decrease in adsorptive performance of the produced MAC is also expected. Hence, the selection of best materials involves compromise between adsorption capacity and rapid and effective magnetic separation.

The produced WPAC demonstrated CBZ removal percentages above 90% for 25 and 50 mg L^{-1} WPAC dosages, which is indicative of its high adsorptive performance. As for the performance of MP1 in CBZ adsorption, their contribution is neglectable. For *in-situ* MAC, increasingly iron salt weight content from MAC2-MP1 to MAC6-MP1 revealed a decrease in the CBZ removal percentage from 91% to 36% (50 mg L^{-1}) which can be explained by S_{BET} reduction and increasingly pore constraints as observed in SEM images.

Carbamazepine removal percentages for MAC4-MP1 and MAC4-MP2 at 50 mg L^{-1} along with the VSM results (section III-1.4) are indicators of the overall better properties of MAC derived from MP1 iron salt ratio.

Rapid and effective magnetic separation was only obtained for MAC6-MP1, MAC4-MP1, MAC3-MP1 and MACX1-MP1, and therefore the selection was limited to these

materials. Even though MAC2-MP1 presented the highest S_{BET} out of all the produced MAC (Table 7), which translated into a CBZ removal percentage comparable to WPAC (Table 11), the magnetic separation from solution was not achieved immediately, hence the reason for not being selected.

Attending to the results in Table 11, MAC4-MP1 and MACX1-MP1 were selected as the two best materials for their performances at 25 mg L^{-1}. MAC3-MP1 was ruled out due to the similar performance with MAC4-MP1 at 50 mg L^{-1}, therefore the decision was to select the material with greater magnetic properties (MAC4-MP1). MAC4-MP1 and MACX1-MP1 provided the best balance between adsorptive performance and immediate magnetic separation, thus being selected for adsorption kinetic (at 25 mg L^{-1}) and equilibrium studies.

Additionally, all produced MAC derived from WPAC have comparable or higher CBZ removal percentages at 50 mg L^{-1} relatively to the commercial derived MCAC2-MP1. Furthermore, MACX1-MP1 has greater performance than the commercial non-magnetic PFFG4, indication the potential of this waste-derived MAC.

Table 11 – Preliminary adsorption results from for the produced materials

Sample	Material dosage (mg L^{-1})	Percentage of CBZ removal (%) Mean ± SD
WPAC	25	95 ± 3
	50	98.9 ± 0.2
MAC2-MP1	50	91 ± 3
MAC3-MP1	50	83 ± 5
MAC4-MP1	25	44 ± 15
	50	79 ± 8
MAC4-MP2	50	63 ± 10
MAC6-MP1	25	15 ± 6
	50	36 ± 8
	75	92 ± 2
MACX1-MP1	25	67 ± 3
	50	92 ± 3
MP1	25	no removal
	50	no removal
MCAC2-MP1	50	41 ± 4
PBFG4	25	62 ± 2

2.3 | Kinetic adsorption study

MAC4-MP1 and MACX1-MP1 were subject of kinetic adsorption studies to determine the time needed to the attainment of equilibrium for CBZ at the interface between the MAC surface and the bulk solution. As previously stated, kinetics of adsorption is essential in the evaluation of the applicability of an adsorbent.

The graphic representation of CBZ adsorption at a given time (q_t, mg g^{-1}) *versus* incubation time in ultrapure water and WWTP effluent, for MAC4-MP1, MACX1-MP1 and WPAC is displayed in Figure 15, along with the best fitting model (pseudo-second order kinetics model). The parameters calculated from fitting of the experimental data to pseudo-first and pseudo-second kinetic models are described in Table 12.

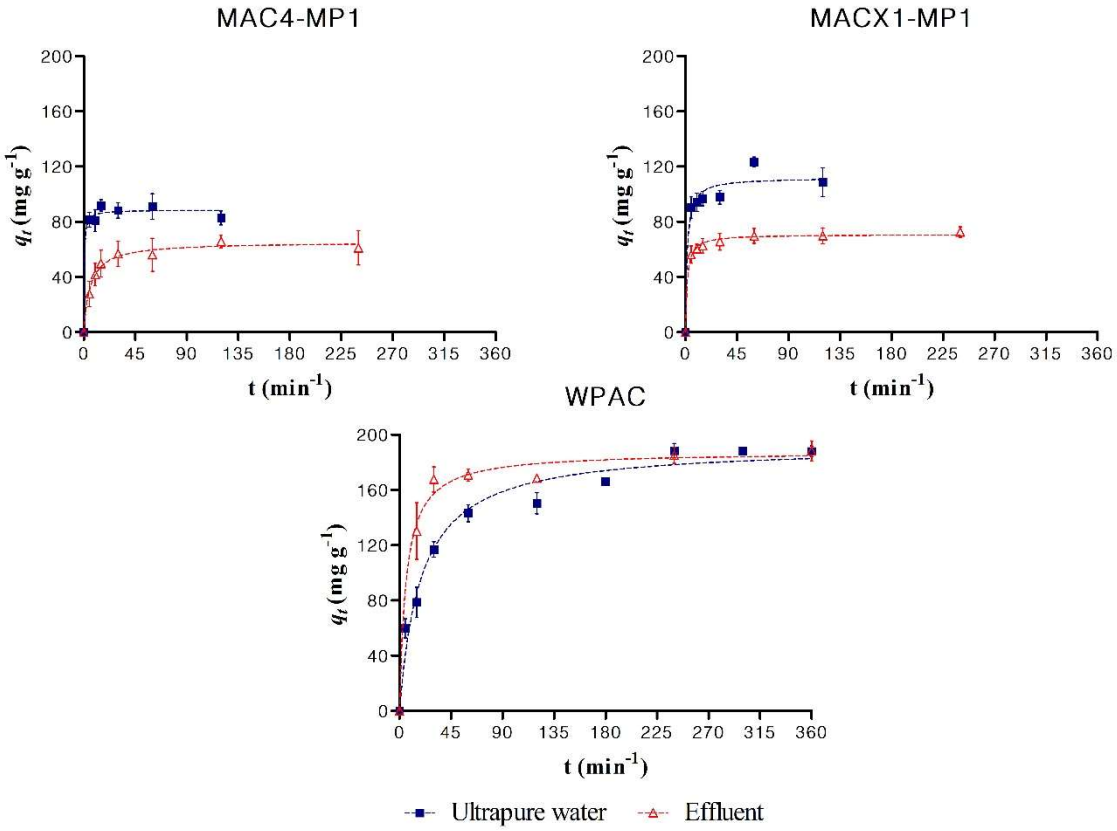

Figure 15 – Experimental data representation for the adsorption of CBZ onto MAC4-MP1, MACX1-MP1 (25 mg L^{-1}) and WPAC (20 mg L^{-1}) [105] in ultrapure (■) and WWTP effluent (Δ), and the corresponding best fitting non-linear kinetic model (pseudo-second order model)

The coefficient of determination values ($R^2 \geq 0.94$) indicate that the experimental data is reasonably described by both pseudo-first and pseudo-second models. According to the

R^2, $S_{y/x}$ and ASS it can be stated that the pseudo-second model better describes the adsorption for the analysed materials. This model assumes that chemical adsorption is the rate limiting step.

Table 12 – Kinetic parameters for the experimental data modelling of the adsorption of CBZ onto MAC4-MP1, MACX1-MP1 and WPAC in ultrapure and WWTP effluent

Matrix	Material	Kinetic model	Model parameters	Fitting parameters		
				R^2	$S_{y/x}$	ASS
Ultrapure water	MAC4-MP1	P1O	q_e = 87 ± 2 k_1 = 0.5 ± 0.1	0.986	4.274	91.32
		P2O	**q_e = 89 ± 3** **k_2 = 0.03 ± 0.02**	**0.986**	**4.213**	**88.76**
	MACX1-MP1	P1O	q_e = 106 ± 5 k_1 = 0.3 ± 0.1	0.945	10.32	532.5
		P2O	**q_e = 112 ± 5** **k_2 = 0.01 ± 0.03**	**0.965**	**8.196**	**335.9**
	WPAC*	P1O	q_e = 175 ± 7 k_1 = 0.038 ±0.007	0.940	16.60	-
		P2O	**q_e = 192 ± 7** **k_2 = 0.00027 ± 0.00005**	**0.974**	**10.81**	-
WWTP effluent	MAC4-MP1	P1O	q_e = 60 ± 1 k_1 = 0.12 ± 0.01	0.984	2.942	51.93
		P2O	**q_e = 65 ± 2** **k_2 = 0.0027 ± 0.0005**	**0.985**	**2.890**	**50.12**
	MACX1-MP1	P1O	q_e = 67 ± 2 k_1 = 0.32 ± 0.06	0.979	3.720	83.05
		P2O	**q_e = 70.8 ± 0.9** **k_2 = 0.009 ± 0.001**	**0.996**	**1.650**	**16.34**
	WPAC*	P1O	q_e = 179 ± 4 k_1 = 0.09 ± 0.01	0.989	7.59	-
		P2O	**q_e = 188 ± 5** **k_2 = 0.0009 ± 0.0002**	**0.990**	**7.22**	-

P1O – pseudo-first order; P2O – pseudo-second order; q_e (mg g^{-1}); k_1 (min^{-1}); k_2 (g mg^{-1} min^{-1})

*Results from Silva et al. (2019) [105]

From the analysis of the graphical representations depicted in Figure 15, it is possible to conclude that the equilibrium was reached for both magnetic materials at around 30-45 minutes, which is slightly faster than the precursor WPAC (60-120 min). According to the pseudo-second and pseudo-first model rate constants (k_2 and k_1), adsorption was faster for the magnetic materials in both matrices by comparison with WPAC. In ultrapure water, MAC4-MP1 presented faster kinetics than MACX1-MP1, while in the WWTP effluent, the opposite trend was verified.

WPAC and MACX1-MP1 kinetic rate constants remain in the same order of magnitude from ultrapure water to effluent, which can indicate no substantial impact of matrix in the kinetics of both materials. Considering k_2 for MAC4-MP1, the adsorption is approximately ten times slower in WWTP effluent.

2.4 | Equilibrium adsorption study

Once it was verified that MAC4-MP1 and MACX1-MP1 have quick equilibrium times for CBZ adsorption, equilibrium adsorption studies were performed also in ultrapure water and WWTP effluent. Figure 16 presents the graphical representation of the amount of CBZ adsorbed at equilibrium (q_e, mg g^{-1}) *versus* the CBZ concentration left in solution (C_e, mg L^{-1}) for MAC4-MP1, MACX1-MP1 and WPAC in both matrices. In Table 13, the resulting parameters from Langmuir and Freundlich isotherm model fittings are listed.

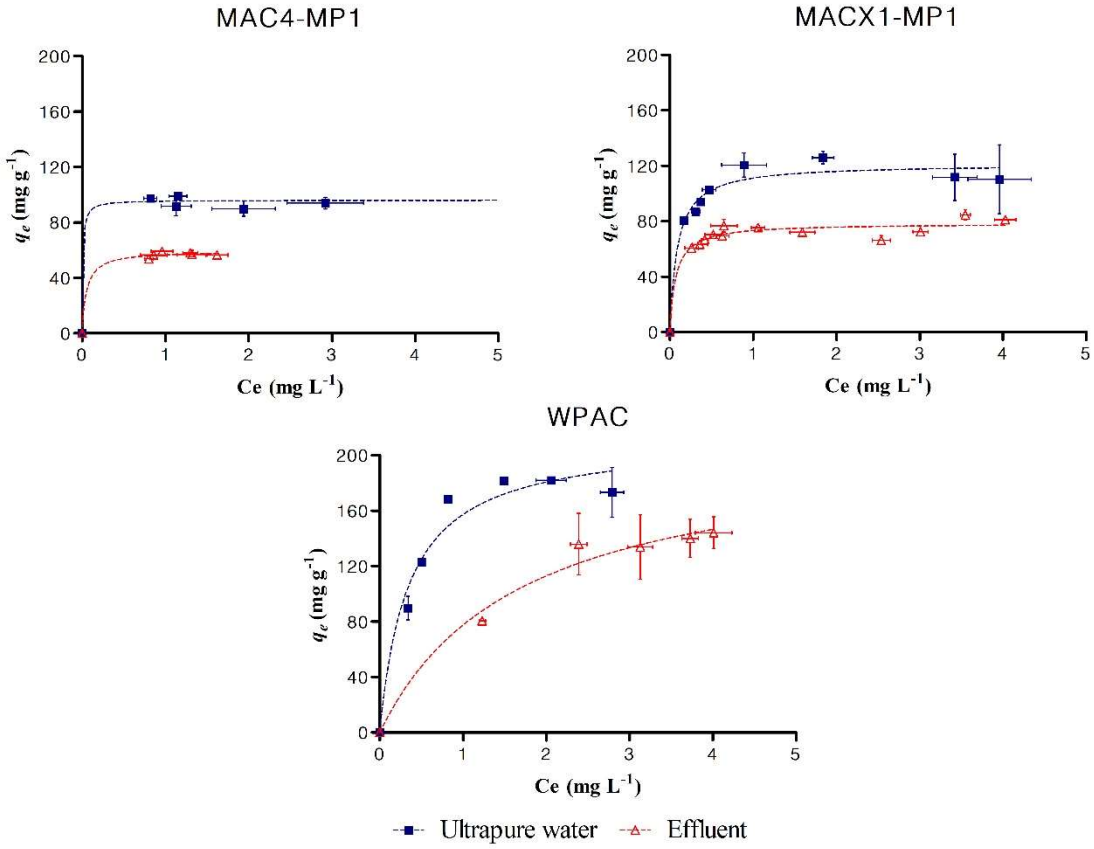

Figure 16 – Experimental data representation for the adsorption of CBZ onto MAC4-MP1, MACX1-MP1 and WPAC [105] in ultrapure (■) and WWTP effluent (Δ), and the corresponding the best fitting non-linear equilibrium model (Langmuir model)

Table 13 – Langmuir and Freundlich isotherm fitting parameters to the experimental data of the adsorption of CBZ onto MAC4-MP1, MACX1-MP1 and WPAC [105] in ultrapure water and WWTP effluent

Matrix	Sample	Isotherm model	Model parameters	Fitting parameters		
				R^2	$S_{y/x}$	ASS
Ultrapure water	MAC4-MP1	**Langmuir**	**q_m = 90 ± 4** **K_L = 115 ± 726**	**0.988**	**4.463**	**99.59**
		Freundlich	K_F = 95 ± 2 n = 57 ± 95	0.988	4.324	93.49
	MACX1-MP1	**Langmuir**	**q_m = 121 ± 5** **K_L = 11 ± 3**	**0.966**	**7.432**	**386.7**
		Freundlich	K_F = 106 ± 4 n = 10 ± 3	0.934	10.39	756.2
	WPAC*	**Langmuir**	**q_m = 212 ± 16** **K_L = 2.8 ± 0.8**	**0.965**	**13.73**	-
		Freundlich	K_F = 149 ± 8 n = 4 ± 1	0.928	19.84	-
WWTP effluent	MAC4-MP1	**Langmuir**	**q_m = 60 ± 3** **K_L = 19 ± 21**	**0.995**	**1.684**	**14.18**
		Freundlich	K_F = 56.6 ± 0.8 n = 26 ± 32	0.995	1.728	14.92
	MACX1-MP1	**Langmuir**	**q_m = 78 ± 2** **K_L = 14 ± 4**	**0.953**	**4.768**	**250.1**
		Freundlich	K_F = 71 ± 1 n = 14 ± 4	0.948	5.003	275.3
	WPAC*	**Langmuir**	**q_m = 209 ± 27** **K_L = 0.6 ± 0.2**	**0.984**	**8.12**	-
		Freundlich	K_F = 82 ± 10 n = 2.3 ± 0.5	0.975	10.03	-

q_m (mg g^{-1}); K_L (L mg^{-1}); K_F (mg$^{1-1/n}$ L$^{1/n}$ g^{-1})

*Results from Silva et al. (2019) [105]

Both isothermal models satisfactorily fit the experimental data ($R^2 \geq 0.92$). According to the error parameters, the best fit was achieved using the Langmuir model in all materials for both matrices, with exception of MAC4-MP1 for ultrapure water where $S_{y/x}$ and ASS parameters where slightly lower for the Freundlich model fitting. Nevertheless, for maximum adsorption capacity (q_m, mg g^{-1}) comparison and given the proximity of the fitting error parameters, the Langmuir model is considered equally valid in the description of MAC4-MP1 experimental equilibrium data in ultrapure water and will be considered in the subsequent discussion. The Langmuir model is often associated with a homogenous adsorption process characterized by a solute monolayer. The separation

factor (R_L) for the presented materials in both matrices was calculated and found to be $0 < R_L < 1$, which indicates favourable CBZ adsorption in all cases.

Comparing q_m in ultrapure water and effluent, the *ex-situ* MAC has higher q_m than MAC4-MP1 in both cases. The MAC4-MP1 has approximately 26% and 24% lower q_m than MACX1-MP1 in ultrapure and WWTP effluent, respectively. This difference can be explained by their distinct $S_{BET.}$ MACX1-MP1 (778 m^2 g^{-1}) has around 29% more surface area than MAC4-MP1 (556 m^2 g^{-1}). This correlation is explained by the fact that S_{BET} strongly influences adsorption, hence differences in S_{BET} values can be directly associated with differences in adsorption capacity.

A decrease in adsorption capacity in both matrices when comparing the magnetic materials with the non-magnetic WPAC is also clearly observed. This can be related to the magnetic nanoparticle occupation of spaces in the complex microporous structure of MAC, possibly leading to pore blockage. Additionally, given the neglectable contribution of the MP to the adsorption of CBZ (section III-2.2), the introduction of an inactive material, in terms of adsorption, into the structure of WPAC ultimately implies a decrease in performance.

A reduction in q_m from ultrapure to effluent is observed for MAC4-MP1 and MACX1-MP1 by 33% and 36%, respectively. This decrease in adsorption capacity, when using WWTP effluent as matrix, can be due to its complex composition, organic matter content and the possibility of competing species that also adsorb onto the AC. Also, given the importance of electrostatic interaction in the adsorption process, the pH of the aqueous phase is a determinant parameter to take into account in this analysis. The pH of the collected effluent was 8.07 and considering the PZC of MAC4-MP1 (~ 6.0) and MACX1-MP1 (~ 5.7) and the pk_a values of CBZ (pk_{a1} = 2.3 [109] and pk_{a2} = 13.9 [110]) it is expected that the surface of the magnetic adsorbents is mainly deprotonated and negatively charged, and that CBZ has neutral net charge. Hence, no electrostatic repulsion between the MAC surface and CBZ exists, which implies that the effluent pH is not expected to negatively impact the adsorption capacity of the MAC in this matrix.

To further evaluate the effect of pH in the adsorption process, a batch adsorption test was performed in ultrapure water at the same incubation conditions of the equilibrium studies, using 25 mg L^{-1} of material, at the effluent pH (~ 8.0) as described in section II-5.4. Table 14 presents CBZ removal percentages for MAC4-MP1 and MACX1-MP1 in ultrapure

water (estimated pH of 5.5-6.0), buffered ultrapure water at the pH of the effluent and WWTP effluent. Results for WPAC are also presented for comparison purposes.

Considering the removal percentages of MAC4-MP1 and MACX1-MP1, results are, as already verified, lower for WWTP effluent. When analysing the results between the two ultrapure water matrices, they are noticeably lower for the buffered ultrapure water (pH ~ 8.0). Attending to both matrices pH, the PZC of the MAC resembles the pH of ultrapure water (~ 5.5-6.0), whereas the pH of the buffered ultrapure water (~ 8.0) is higher. This means the distribution of charges in the surface of the MAC might be different in both matrices. Negative and positive charges should be equality distributed on MAC4-MP1 and MACX1-MP1 surfaces in ultrapure water (pH = PCZ) whereas, as stated before, their surfaces are predominantly negative at pH ~ 8.0 (buffered ultrapure water and WWTP effluent). Although, no electrostatic repulsion occurs between CBZ and MAC surface at the referred pH conditions, these differences in surface charges distribution might influence adsorption and explain the results from Table 14. Additionally, the buffered ultrapure water and WWTP effluent present significantly higher ionic strength when compared to the non-buffered ultrapure water. Ionic strength is known to strongly influence adsorption and can also be the cause of the verified decrease in adsorptive performance.

Overall, the adsorption capacity decline in WWTP effluent can possibly be explained be cumulative effect of several factors including the complexity of composition, the organic matter content, the existence of competing species, the pH and the ionic strength.

Table 14 – CBZ removal percentages for the selected best MAC and WPAC in ultrapure water, buffered ultrapure water and WWTP effluent

Material	**Percentage of CBZ removal (%) at 25 mg L^{-1}** Mean ± SD		
	Ultrapure water (pH ~ 5.5-6.0)	**Ultrapure water** (pH ~ 8.0)	**WWTP effluent** (pH ~ 8.0)
MAC4-MP1	48 ± 2	35 ± 4	15 ± 3
MACX1-MP1	64 ± 3	44 ± 2	38 ± 2
WPAC	95 ± 3	93 ± 2	-

Despite the inferior maximum adsorption capacity of MAC4-MP1 and MACX1-MP1 for CBZ when compared to the non-magnetic WPAC, their performance is still, in some cases, comparable to commercial non-magnetic PAC. In Calisto et al. (2015) [78], adsorption equilibrium studies for CBZ removal from ultrapure water for the commercial PAC PBFG4 revealed a q_m of 116 ± 3 mg g^{-1}, which is inferior to MACX1-MP1 (121 ± 5 mg g^{-1}) and only slightly superior to MAC4-MP1 (90 ± 4 mg g^{-1}). This highlights the competitiveness of the produced MAC with the advantage of easy magnetic retrievability from solution.

However, there is still a gap in the adsorptive performance between MAC and high performance commercial non-magnetic PAC. In Silva et al. (2019) [105], a commercial PAC presented overall higher q_m for CBZ removal in both ultrapure water (174 ± 4 mg g^{-1}) and effluent (160 ± 7 mg g^{-1}) comparing to the produced MAC in this work. The performance gap between magnetic and non-magnetic PAC can be reduced by reducing the ratio of magnetic particles, that inevitably damage adsorptive performance, in relation to PAC, while maintaining effective retrievability. An exhaustive optimization of MAC synthesis conditions in order to maximize the precipitation of magnetic iron oxides, in detriment to the non-magnetic, might provide means for that.

To the best of the author's knowledge, there is only one literature study applying a magnetically retrievable PAC, prepared in an *ex-situ* approach, for the CBZ adsorption from real WWTP effluent [96]. The produced MAC (S_{BET} = 1241 m^2 g^{-1}) revealed a q_m of 182.9 mg g^{-1}, inevitably inferior to its commercial PAC precursor, but with a great balance between performance competitiveness and magnetic properties.

Nonetheless, the results for CBZ removal by MAC4-MP1 and MACX1-MP1 from ultrapure water (90 ± 4 mg g^{-1} and 121 ± 5 mg g^{-1}, respectively) and from effluent (60 ± 3 mg g^{-1} and 78 ± 2 mg g^{-1}, respectively) point to the promising application of magnetically retrievable WPAC in continuous water treatment systems.

IV. Conclusion

Considering the WWTP incapacity to effectively remove pharmaceuticals from wastewater using conventional treatments, the use of PAC in continuous water treatment adsorption systems provides an alternative, versatile, and efficient technology for effluent refinement. The use of PS to produce WPAC constitutes the upcycling of an industrial waste into a value-added product, which enforces the principles of a circular economy. However, PAC separation from the treated aqueous phase is hampered by its small particle size.

To overcome this issue, magnetically retrievable WPAC were successfully produced *via* two synthesis routes, namely the *in-situ* and the *ex-situ* routes, through the coprecipitation of magnetic iron oxides. The produced MAC inevitably have lower S_{BET}, V_p and W_0 than the precursor WPAC. Nonetheless, the *ex-situ* (S_{BET} = 777 $m^2\ g^{-1}$) and the *in-situ* materials (S_{BET} = 449 - 805 $m^2\ g^{-1}$) presented properties comparable to a non-magnetic commercial PAC (PBFG4 – 848 $m^2\ g^{-1}$), with the advantage of viable magnetic separation from solution. Magnetic properties of the produced MAC were concluded to be caused by the presence of magnetite and maghemite.

In what concerns adsorptive performance, preliminary adsorption studies in ultrapure water indicated that increasingly iron salt proportions for the *in-situ* MAC corresponded to poorer adsorptive removals. Two MAC materials – MAC4-MP1 and MACX1-MP1 – were selected for maximizing adsorptive performance and immediate magnetic retrievability. These materials were subjected to extensive adsorption studies.

From kinetic and equilibrium studies in ultrapure and WWTP effluent it was possible to conclude that:

1) Both MAC4-MP1 and MACX1-MP1 have faster kinetics than their precursor WPAC (60-120 min), achieving equilibrium at 30-45 min of incubation, in both matrices.
2) In ultrapure water, both selected MAC materials presented around 35% higher maximum adsorption capacities than in WWTP effluent and that discrepancy can be associated with the presence of competing species, pH and ionic strength variations, complexity of the matrix (e.g. organic matter content).
3) Considering both matrices, MACX1-MP1 has approximately 25% higher q_m than MAC4-MP1, which can be attributed to differences in S_{BET}.

4) The produced MAC have q_m values for CBZ in ultrapure water which are higher (MACX1-MP1 – 121 ± 5 mg g^{-1}) or comparable (MAC4-MP1 – 90 ± 4 mg g^{-1}) to a commercial non-magnetic PAC (PBFG4 – 116 ± 3 mg g^{-1}) which highlight the competitiveness of these materials with advantageous magnetic properties.
5) Results from adsorption WWTP effluent - MAC4-MP1 (60 ± 3 mg g^{-1}) and MACX1-MP1 (78 ± 2 mg g^{-1}) – are excellent indicators of the potential application of magnetically retrievable PAC in the refinement of wastewaters.

Overall, this work concludes that the adsorption of CBZ onto waste-based MAC is not only viable in both ultrapure and real WWTP but can, in some cases, be comparable or higher to the performance of non-magnetic commercial PAC. Still, further optimization work is required in order to minimize the inevitable impact of imparting magnetic properties to PAC.

V. References

[1] A.G. Kostianoy, J. De Boer, P. Garrigues, J. Gu, K.C. Jones, T. Knepper, A. Newton, D.L. Sparks, The Handbook of Environmental Chemistry - Waste Water Treatment and Reuse in the Mediterranean region, 2011.

[2] T. Deblonde, C. Cossu-Leguille, P. Hartemann, Emerging pollutants in wastewater: A review of the literature, Int. J. Hyg. Environ. Health. 214 (2011).

[3] N.H. Tran, M. Reinhard, K.Y.H. Gin, Occurrence and fate of emerging contaminants in municipal wastewater treatment plants from different geographical regions-a review, Water Res. 133 (2018) 182–207.

[4] R.U. Halden, Epistemology of contaminants of emerging concern and literature meta-analysis, J. Hazard. Mater. 282 (2015) 2–9.

[5] European Parliament, Directive 2013/39/EU of the European Parliament and of the Council of 12 August 2013 amending Directives 2000/60/EC and 2008/105/EC as regards priority substances in the field of water policy, Brussels, 2013.

[6] European Commission, Decision 2015/495/EU of 20 March 2015 establishing a watch list of substances for Union-wide monitoring in the field of water policy pursuant to Directive 2008/ 105/ EC of the European Parliament and of the Council, Brussels, 2015.

[7] European Commission, Decision 2018/840/EU of 5 June 2018 establishing a watch list of substances for Union-wide monitoring in the field of water policy pursuant to Directive 2008/105/EC of the European Parliament and of the Council and repealing Commission Implementing Deci, Brussels, 2018.

[8] A. Jelic, M. Petrović, D. Barcelo, Pharmaceuticals in Drinking Water, in: D. Barcelo (Ed.), Handb. Environ. Chem. - Emerg. Org. Contam. Hum. Heal., vol. 20, Springer, 2012: pp. 47–70.

[9] C.P. Silva, G. Jaria, M. Otero, V.I. Esteves, V. Calisto, Waste-based alternative adsorbents for the remediation of pharmaceutical contaminated waters: Has a step forward already been taken?, Bioresour. Technol. 250 (2018) 888–901.

[10] S.D. Richardson, Environmental mass spectrometry: Emerging contaminants and current issues, Anal. Chem. 84 (2012) 747–778.

[11] J. Rivera-Utrilla, M. Sánchez-Polo, M.Á. Ferro-García, G. Prados-Joya, R. Ocampo-Pérez, Pharmaceuticals as emerging contaminants and their removal from water. A review, Chemosphere. 93 (2013) 1268–1287.

[12] S.D. Richardson, Environmental Mass Spectrometry: Emerging Contaminants and Current Issues, Anal. Chem. 82 (2010) 4742–4774.

[13] T. Heberer, Occurrence, fate, and removal of pharmaceutical residues in the

aquatic environment: A review of recent research data, Toxicol. Lett. 131 (2002) 5–17.

[14] M.S.U. Rehman, N. Rashid, M. Ashfaq, A. Saif, N. Ahmad, J.I. Han, Global risk of pharmaceutical contamination from highly populated developing countries, Chemosphere. 138 (2015) 1045–1055.

[15] B. Halling-Sørensen, S. Nors Nielsen, P.F. Lanzky, F. Ingerslev, H.C. Holten Lützhøft, S.E. Jørgensen, Occurrence, fate and effects of pharmaceutical substances in the environment- A review, Chemosphere. 36 (1998) 357–393.

[16] A. Jelic, M. Gros, A. Ginebreda, R. Cespedes-Sánchez, F. Ventura, M. Petrovic, D. Barcelo, Occurrence, partition and removal of pharmaceuticals in sewage water and sludge during wastewater treatment, Water Res. 45 (2011) 1165–1176.

[17] Y. Luo, W. Guo, H.H. Ngo, L.D. Nghiem, F.I. Hai, J. Zhang, S. Liang, X.C. Wang, A review on the occurrence of micropollutants in the aquatic environment and their fate and removal during wastewater treatment, Sci. Total Environ. 473–474 (2014) 619–641.

[18] C.G. Daughton, I.S. Ruhoy, Environmental footprint of pharmaceuticals: The significance of factors beyond direct excretion to sewers, Environ. Toxicol. Chem. 28 (2009) 2495–2521.

[19] I. Michael, L. Rizzo, C.S. McArdell, C.M. Manaia, C. Merlin, T. Schwartz, C. Dagot, D. Fatta-Kassinos, Urban wastewater treatment plants as hotspots for the release of antibiotics in the environment: A review, Water Res. 47 (2013) 957–995.

[20] T.M. Scott, P.J. Phillips, D.W. Kolpin, K.M. Colella, E.T. Furlong, W.T. Foreman, J.L. Gray, Pharmaceutical manufacturing facility discharges can substantially increase the pharmaceutical load to U.S. wastewaters, Sci. Total Environ. 636 (2018) 69–79.

[21] S. Kleywegt, M. Payne, F. Ng, T. Fletcher, Environmental loadings of Active Pharmaceutical Ingredients from manufacturing facilities in Canada, Sci. Total Environ. 646 (2019) 257–264.

[22] O. Cardoso, J.M. Porcher, W. Sanchez, Factory-discharged pharmaceuticals could be a relevant source of aquatic environment contamination: Review of evidence and need for knowledge, Chemosphere. 115 (2014) 20–30.

[23] D.G.G.J. Larsson, C. de Pedro, N. Paxeus, Effluent from drug manufactures contains extremely high levels of pharmaceuticals, J. Hazard. Mater. 148 (2007) 751–755.

[24] P.K. Thai, L.X. Ky, V.N. Binh, P.H. Nhung, P.T. Nhan, N.Q. Hieu, N.T.T. Dang, N.K.B. Tam, N.T.K. Anh, Occurrence of antibiotic residues and antibiotic-resistant bacteria in effluents of pharmaceutical manufacturers and other sources around Hanoi, Vietnam, Sci. Total Environ. 645 (2018) 393–400.

[25] T. aus der Beek, F.A. Weber, A. Bergmann, S. Hickmann, I. Ebert, A. Hein, A. Küster, Pharmaceuticals in the environment-Global occurrences and perspectives, Environ. Toxicol. Chem. 35 (2016) 823–835.

[26] F. Desbiolles, L. Malleret, C. Tiliacos, P. Wong-Wah-Chung, I. Laffont-Schwob, Occurrence and ecotoxicological assessment of pharmaceuticals: Is there a risk for the Mediterranean aquatic environment?, Sci. Total Environ. 639 (2018) 1334–1348.

[27] Q. Sui, X. Cao, S. Lu, W. Zhao, Z. Qiu, G. Yu, Occurrence, sources and fate of pharmaceuticals and personal care products in the groundwater: A review, Emerg. Contam. 1 (2015) 14–24.

[28] T. Heberer, Tracking persistent pharmaceutical residues from municipal sewage to drinking water, J. Hydrol. 266 (2002) 175–189.

[29] V. de Jesus Gaffney, C.M.M. Almeida, A. Rodrigues, E. Ferreira, M.J. Benoliel, V.V. Cardoso, Occurrence of pharmaceuticals in a water supply system and related human health risk assessment, Water Res. 72 (2015) 199–208.

[30] A.M.P.T. Pereira, L.J.G. Silva, C.S.M. Laranjeiro, L.M. Meisel, C.M. Lino, A. Pena, Human pharmaceuticals in Portuguese rivers: The impact of water scarcity in the environmental risk, Sci. Total Environ. 609 (2017) 1182–1191.

[31] M. Cleuvers, Aquatic ecotoxicity of pharmaceuticals including the assessment of combination effects, Toxicol. Lett. 142 (2003) 185–194.

[32] A. Kumar, I. Xagoraraki, Human health risk assessment of pharmaceuticals in water: An uncertainty analysis for meprobamate, carbamazepine, and phenytoin, Regul. Toxicol. Pharmacol. 57 (2010) 146–156.

[33] E.J. Han, D.S. Lee, Significance of metabolites in the environmental risk assessment of pharmaceuticals consumed by human, Sci. Total Environ. 592 (2017) 600–607.

[34] M.I. Vasquez, A. Lambrianides, M. Schneider, K. Kümmerer, D. Fatta-Kassinos, Environmental side effects of pharmaceutical cocktails: What we know and what we should know, J. Hazard. Mater. 279 (2014) 169–189.

[35] F. Pomati, C.J. Cotsapas, S. Castiglioni, E. Zuccato, D. Calamari, Gene expression profiles in zebrafish (Danio rerio) liver cells exposed to a mixture of

pharmaceuticals at environmentally relevant concentrations, Chemosphere. 70 (2007) 65–73.

[36] F. Pomati, S. Castiglioni, E. Zuccato, R. Fanelli, D. Vigetti, C. Rossetti, D. Calamari, Effects of a complex mixture of therapeutic drugs at environmental levels on human embryonic cells, Environ. Sci. Technol. 40 (2006) 2442–2447.

[37] M. Schmitz, M. Beghin, S.N.M. Mandiki, K. Nott, M. Gillet, S. Ronkart, C. Robert, S. Baekelandt, P. Kestemont, Environmentally-relevant mixture of pharmaceutical drugs stimulates sex-steroid hormone production and modulates the expression of candidate genes in the ovary of juvenile female rainbow trout, Aquat. Toxicol. 205 (2018) 89–99.

[38] B. Tiwari, B. Sellamuthu, Y. Ouarda, P. Drogui, R.D. Tyagi, G. Buelna, Review on fate and mechanism of removal of pharmaceutical pollutants from wastewater using biological approach, Bioresour. Technol. 224 (2017) 1–12.

[39] M. Gros, M. Petrović, A. Ginebreda, D. Barceló, Removal of pharmaceuticals during wastewater treatment and environmental risk assessment using hazard indexes, Environ. Int. 36 (2010) 15–26.

[40] A. Bahlmann, W. Brack, R.J. Schneider, M. Krauss, Carbamazepine and its metabolites in wastewater: Analytical pitfalls and occurrence in Germany and Portugal, Water Res. 57 (2014) 104–114.

[41] S.K. Behera, H.W. Kim, J.-E. Oh, H.-S. Park, Occurrence and removal of antibiotics, hormones and several other pharmaceuticals in wastewater treatment plants of the largest industrial city of Korea, Sci. Total Environ. 409 (2011) 4351–4360.

[42] Y. Zhang, S.U. Geißen, C. Gal, Carbamazepine and diclofenac: Removal in wastewater treatment plants and occurrence in water bodies, Chemosphere. 73 (2008) 1151–1161.

[43] A.M.P.T. Pereira, L.J.G. Silva, L.M. Meisel, C.M. Lino, A. Pena, Environmental impact of pharmaceuticals from Portuguese wastewaters: Geographical and seasonal occurrence, removal and risk assessment, Environ. Res. 136 (2015) 108–119.

[44] R.C. Bansal, M. Goyal, Activated carbon adsorption, Taylor & Francis, 2005.

[45] H. Marsh, F. Rodríguez-Reinoso, Activated carbon, Elsevier, 2006.

[46] C. Moreno-Castilla, Adsorption of organic molecules from aqueous solutions on carbon materials, Carbon N. Y. 42 (2004) 83–94.

[47] K.Y. Foo, B.H. Hameed, Insights into the modeling of adsorption isotherm

systems, Chem. Eng. J. 156 (2010) 2–10.

[48] S. Brunauer, P.H. Emmett, E. Teller, Adsorption of Gases in Multimolecular Layers, J. Am. Chem. Soc. 60 (1938) 309–319.

[49] H. Marsh, B. Rand, The characterization of microporous carbons by means of the dubinin-radushkevich equation, J. Colloid Interface Sci. 33 (1970) 101–116.

[50] M.C. Ncibi, Applicability of some statistical tools to predict optimum adsorption isotherm after linear and non-linear regression analysis, J. Hazard. Mater. 153 (2008) 207–212.

[51] C.H. Giles, T.H. MacEwan, S.N. Nakhwa, D. Smith, Studies in adsorption. Part XI. A system of classification of solution adsorption isotherms, and its use in diagnosis of adsorption mechanisms and in measurement of specific surface areas of solids, J. Chem. Soc. (1960) 3973.

[52] H. Butt, K. Graf, M. Kappl, Physics and Chemistry of Interfaces, Wiley, 2003.

[53] H. Qiu, Q. Zhang, L. Lv, B. Pan, W. Zhang, Q. Zhang, Critical review in adsorption kinetic models, J. Zhejiang Univ. A. 10 (2009) 716–724.

[54] T.J. Bandosz, Activated carbon surfaces in environmental remediation, Elsevier, 2006.

[55] F. Çeçen, O. Aktaş, Activated carbon for water and wastewater treatment : integration of adsorption and biological treatment, Wiley-VCH, 2012.

[56] S.-H. Jung, S.-J. Oh, G.-G. Choi, J.-S. Kim, Production and characterization of microporous activated carbons and metallurgical bio-coke from waste shell biomass, J. Anal. Appl. Pyrolysis. 109 (2014) 123–131.

[57] J.F. González, S. Román, J.M. Encinar, G. Martínez, Pyrolysis of various biomass residues and char utilization for the production of activated carbons, J. Anal. Appl. Pyrolysis. 85 (2009) 134–141.

[58] C. Namasivayam, D. Sangeetha, Recycling of agricultural solid waste, coir pith: Removal of anions, heavy metals, organics and dyes from water by adsorption onto ZnCl2 activated coir pith carbon, J. Hazard. Mater. 135 (2006) 449–452.

[59] J. Sreńscek-Nazzal, W. Kamińska, B. Michalkiewicz, Z.C. Koren, Production, characterization and methane storage potential of KOH-activated carbon from sugarcane molasses, Ind. Crops Prod. 47 (2013) 153–159.

[60] F. Kaouah, S. Boumaza, T. Berrama, M. Trari, Z. Bendjama, Preparation and characterization of activated carbon from wild olive cores (oleaster) by H3PO4 for the removal of Basic Red 46, J. Clean. Prod. 54 (2013) 296–306.

[61] J. Hayashi, T. Horikawa, I. Takeda, K. Muroyama, F. Nasir Ani, Preparing activated carbon from various nutshells by chemical activation with K2CO3, Carbon N. Y. 40 (2002) 2381–2386.

[62] J.M. Dias, M.C.M. Alvim-Ferraz, M.F. Almeida, J. Rivera-Utrilla, M. Sánchez-Polo, Waste materials for activated carbon preparation and its use in aqueous-phase treatment: A review, J. Environ. Manage. 85 (2007) 833–846.

[63] P. González-García, Activated carbon from lignocellulosics precursors: A review of the synthesis methods, characterization techniques and applications, Renew. Sustain. Energy Rev. 82 (2018) 1393–1414

[64] O. Ioannidou, A. Zabaniotou, Agricultural residues as precursors for activated carbon production—A review, Renew. Sustain. Energy Rev. 11 (2007) 1966–2005.

[65] A.R. Satayeva, C.A. Howell, A. V. Korobeinyk, J. Jandosov, V.J. Inglezakis, Z.A. Mansurov, S. V. Mikhalovsky, Investigation of rice husk derived activated carbon for removal of nitrate contamination from water, Sci. Total Environ. 630 (2018) 1237–1245.

[66] A.-N.A. El-Hendawy, A.J. Alexander, R.J. Andrews, G. Forrest, Effects of activation schemes on porous, surface and thermal properties of activated carbons prepared from cotton stalks, J. Anal. Appl. Pyrolysis. 82 (2008) 272–278.

[67] Q. Lu, Z. Wang, C. Dong, Z. Zhang, Y. Zhang, Y. Yang, X. Zhu, Selective fast pyrolysis of biomass impregnated with ZnCl2: Furfural production together with acetic acid and activated carbon as by-products, J. Anal. Appl. Pyrolysis. 91 (2011) 273–279.

[68] M.A. Díaz-Díez, V. Gómez-Serrano, C. Fernández González, E.M. Cuerda-Correa, A. Macías-García, Porous texture of activated carbons prepared by phosphoric acid activation of woods, Appl. Surf. Sci. 238 (2004) 309–313.

[69] G. Jaria, C.P. Silva, J.A.B.P. Oliveira, S.M. Santos, M.V. Gil, M. Otero, V. Calisto, V.I. Esteves, Production of highly efficient activated carbons from industrial wastes for the removal of pharmaceuticals from water—A full factorial design, J. Hazard. Mater. 370 (2019) 212–218.

[70] G. Oliveira, V. Calisto, S.M. Santos, M. Otero, V.I. Esteves, Paper pulp-based adsorbents for the removal of pharmaceuticals from wastewater: A novel approach towards diversification, Sci. Total Environ. 631–632 (2018) 1018–1028.

[71] E. Unur, Functional nanoporous carbons from hydrothermally treated biomass for environmental purification, Microporous Mesoporous Mater. 168 (2013) 92–101.

[72] G. Jaria, C.P. Silva, C.I.A. Ferreira, M. Otero, V. Calisto, Sludge from paper mill effluent treatment as raw material to produce carbon adsorbents: An alternative waste management strategy, J. Environ. Manage. 188 (2017) 203–211.

[73] G. Jaria, V. Calisto, C.P. Silva, M.V. Gil, M. Otero, V.I. Esteves, Obtaining granular activated carbon from paper mill sludge – A challenge for application in the removal of pharmaceuticals from wastewater, Sci. Total Environ. 653 (2019) 393–400.

[74] N.. Khalili, J.. Vyas, W. Weangkaew, S.. Westfall, S.. Parulekar, R. Sherwood, Synthesis and characterization of activated carbon and bioactive adsorbent produced from paper mill sludge, Sep. Purif. Technol. 26 (2002) 295–304.

[75] W.-H. Li, Q.-Y. Yue, B.-Y. Gao, X.-J. Wang, Y.-F. Qi, Y.-Q. Zhao, Y.-J. Li, Preparation of sludge-based activated carbon made from paper mill sewage sludge by steam activation for dye wastewater treatment, Desalination. 278 (2011) 179–185.

[76] Y. Li, Q. Yue, W. Li, B. Gao, J. Li, J. Du, Properties improvement of paper mill sludge-based granular activated carbon fillers for fluidized-bed bioreactor by bentonite (Na) added and acid washing, J. Hazard. Mater. 197 (2011) 33–39.

[77] V. Calisto, C.I.A. Ferreira, S.M. Santos, M.V. Gil, M. Otero, V.I. Esteves, Production of adsorbents by pyrolysis of paper mill sludge and application on the removal of citalopram from water, Bioresour. Technol. 166 (2014) 335–344.

[78] V. Calisto, C.I.A. Ferreira, J.A.B.P. Oliveira, M. Otero, V.I. Esteves, Adsorptive removal of pharmaceuticals from water by commercial and waste-based carbons, J. Environ. Manage. 152 (2015) 83–90.

[79] G. Jaria, V. Calisto, M.V. Gil, M. Otero, V.I. Esteves, Removal of fluoxetine from water by adsorbent materials produced from paper mill sludge, J. Colloid Interface Sci. 448 (2015) 32–40.

[80] V. Calisto, G. Jaria, C.P. Silva, C.I.A. Ferreira, M. Otero, V.I. Esteves, Single and multi-component adsorption of psychiatric pharmaceuticals onto alternative and commercial carbons, J. Environ. Manage. 192 (2017) 15–24.

[81] T. Krahnstöver, T. Wintgens, Separating powdered activated carbon (PAC) from wastewater - Technical process options and assessment of removal efficiency, J. Environ. Chem. Eng. 6 (2018) 5744–5762.

[82] M.T.H. Siddiqui, S. Nizamuddin, H.A. Baloch, N.M. Mubarak, M. Al-Ali, S.A. Mazari, A.W. Bhutto, R. Abro, M. Srinivasan, G. Griffin, Fabrication of advance magnetic carbon nano-materials and their potential applications: A review, J. Environ. Chem. Eng. 7 (2018) 102812.

[83] R.M. Cornell, U. Schwertmann, The Iron Oxides Structure, Properties, Reactions, Occurences and Uses, 2nd Editio, Wiley-VCH, 2003.

[84] U. Schwertmann, R.M. Cornell, Iron Oxides in the Laboratory Preparation and Characterization, 2000.

[85] T. Ahn, J.H. Kim, H.M. Yang, J.W. Lee, J.D. Kim, Formation pathways of magnetite nanoparticles by coprecipitation method, J. Phys. Chem. C. 116 (2012) 6069–6076.

[86] K.R. Thines, E.C. Abdullah, N.M. Mubarak, M. Ruthiraan, Synthesis of magnetic biochar from agricultural waste biomass to enhancing route for waste water and polymer application: A review, Renew. Sustain. Energy Rev. 67 (2017) 257–276.

[87] F. Yazdani, M. Seddigh, Magnetite nanoparticles synthesized by co-precipitation method: The effects of various iron anions on specifications, Mater. Chem. Phys. 184 (2016) 318–323.

[88] Y. Tian, M. Wu, X. Lin, P. Huang, Y. Huang, Synthesis of magnetic wheat straw for arsenic adsorption, J. Hazard. Mater. 193 (2011) 10–16.

[89] X. Hu, Z. Ding, A.R. Zimmerman, S. Wang, B. Gao, Batch and column sorption of arsenic onto iron-impregnated biochar synthesized through hydrolysis, Water Res. 68 (2015) 206–216.

[90] X. Zhu, Y. Liu, F. Qian, C. Zhou, S. Zhang, J. Chen, Preparation of magnetic porous carbon from waste hydrochar by simultaneous activation and magnetization for tetracycline removal, Bioresour. Technol. 154 (2014) 209–214.

[91] A.L. Cazetta, O. Pezoti, K.C. Bedin, T.L. Silva, A. Paesano Junior, T. Asefa, V.C. Almeida, Magnetic Activated Carbon Derived from Biomass Waste by Concurrent Synthesis: Efficient Adsorbent for Toxic Dyes, ACS Sustain. Chem. Eng. 4 (2016) 1058–1068.

[92] D. Shan, S. Deng, T. Zhao, B. Wang, Y. Wang, J. Huang, G. Yu, J. Winglee, M.R. Wiesner, Preparation of ultrafine magnetic biochar and activated carbon for pharmaceutical adsorption and subsequent degradation by ball milling, J. Hazard. Mater. 305 (2016) 156–163.

[93] Y. Liu, X. Zhu, F. Qian, S. Zhang, J. Chen, Magnetic activated carbon prepared from rice straw-derived hydrochar for triclosan removal, RSC Adv. 4 (2014) 63620–63626.

[94] Z. Hao, C. Wang, Z. Yan, H. Jiang, H. Xu, Magnetic particles modification of coconut shell-derived activated carbon and biochar for effective removal of phenol from water, Chemosphere. 211 (2018) 962–969.

[95] S.-Y. Gu, C.-T. Hsieh, Y.A. Gandomi, Z.-F. Yang, L. Li, C.-C. Fu, R.-S. Juang, Functionalization of activated carbons with magnetic Iron oxide nanoparticles for removal of copper ions from aqueous solution, J. Mol. Liq. 277 (2018) 499–505.

[96] M. Baghdadi, E. Ghaffari, B. Aminzadeh, Removal of carbamazepine from municipal wastewater effluent using optimally synthesized magnetic activated carbon: Adsorption and sedimentation kinetic studies, J. Environ. Chem. Eng. 4 (2016) 3309–3321.

[97] C.A. Luiz, Oliveira, R.V.R.A. Rios, J.D. Fabris, V. Garg, K. Sapag, R.M. Lago, Activated carbon / iron oxide magnetic composites for the adsorption of contaminants in water, Carbon N. Y. 40 (2002) 2177–2183

[98] A.K. Gupta, M. Gupta, Synthesis and surface engineering of iron oxide nanoparticles for biomedical applications, Biomaterials. 26 (2005) 3995–4021.

[99] F. Reguyal, A.K. Sarmah, W. Gao, Synthesis of magnetic biochar from pine sawdust via oxidative hydrolysis of FeCl2for the removal sulfamethoxazole from aqueous solution, J. Hazard. Mater. 321 (2017) 868–878.

[100] H. Whatley, Basic Principles and Modes of Capillary Electrophoresis, in: J.R. Petersen, A.A. Mohammad (Eds.), Clin. Forensic Appl. Capill. Electrophor., Humana Press, Totowa, NJ, 2001: pp. 21–58.

[101] V. Calisto, Environmental occurrence and fate of psychiatric pharmaceuticals, University of Aveiro, 2011.

[102] J.P. Quirino, A. Wuethrich, Capillary Electrophoresis: Overview, in: P. Worsfold, A. Townshend, C. Poole (Eds.), Encycl. Anal. Sci., 3rd ed., Elsevier Inc., 2018: pp. 334–343.

[103] M. Kosmulski, Isoelectric points and points of zero charge of metal (hydr)oxides: 50 years after Parks' review, Adv. Colloid Interface Sci. 238 (2016) 1–61.

[104] J.N. Miller, J.C. Miller, Statistics and Chemometrics for Analytical Chemistry, 6th ed., Prentice Hall, 2010.

[105] C.P. Silva, G. Jaria, M. Otero, V.I. Esteves, V. Calisto, Adsorption of pharmaceuticals from biologically treated municipal wastewater using paper mill sludge-based activated carbon, Environ. Sci. Pollut. Res. (2019) 1–12.

[106] M. Sevilla, A.B. Fuertes, The production of carbon materials by hydrothermal carbonization of cellulose, Carbon N. Y. 47 (2009) 2281–2289.

[107] M. Balachandran, K. Ag, Study of Stacking Structure of Amorphous Carbon by X-Ray Diffraction Technique, Int. J. Electrochem. Sci. 7 (2012) 3127–3134.

[108] S. Mopoung, P. Moonsri, W. Palas, S. Khumpai, Characterization and Properties of Activated Carbon Prepared from Tamarind Seeds by KOH Activation for Fe(III) Adsorption from Aqueous Solution, Sci. World J. 2015 (2015).

[109] L.D. Nghiem, A.I. Schäfer, M. Elimelech, Pharmaceutical retention mechanisms by nanofiltration membranes., Environ. Sci. Technol. 39 (2005) 7698–705.

[110] O.A.. Jones, N. Voulvoulis, J.. Lester, Aquatic environmental assessment of the top 25 English prescription pharmaceuticals, Water Res. 36 (2002) 5013–5022.